Response to reviewer comments for manuscript number: acp-2019-1052

Comments by reviewers are shown in italic typeface and the responses shown normal typeface.

Referee comments:

Reviewer #1:

The paper uses concurrent observations of sea surface iodide (SSI), ozone (O3), and iodine monoxide (IO) along with several other parameters to assess different methods of estimating iodine fluxes to the marine boundary layer. Region-specific forms of these methods for the Indian Ocean and Southern Ocean are derived and further assessed against the observations. The results are substantially different in the Indian Ocean and Southern Ocean and on either side of the polar front. Furthermore, the results are often contrary to previous findings, highlighting the need for further studies.

The fundamental finding of the paper that existing methods fail to reproduce observations and that consistent improvements applicable to the full data set are not forthcoming is worthy of publication; however, the authors must better demonstrate and communicate this with robust statistical tests. Toward this point I have the following specific major comments:

RESPONSE: We thank the reviewer for providing detailed constructive comments and suggestions. The following is a point by point response to the review with corresponding changes made to the manuscript. We hope that the manuscript will now be acceptable with these changes.

1) As the title states the observational region encompasses the Indian Ocean and Southern Ocean, however, analysis of (SSI) in the Indian Ocean alone fails to obtain a significant result. As the authors state this is likely due to the limited statistics (N=18).
This finding calls into question whether the application of the combined fitted result should be applicable to the Indian Ocean. ANOVA or similar methods should be applied to determine whether the Indian Ocean is statistically different. In particular, an F-test should be conducted. The presented results suggest that spatial and temporal differences between the measurement campaigns, and other effects may present confounding variables to such methods. Despite this, even "failed" statistical tests with inconclusive results are needed for proper framing of the results in the Indian Ocean.

RESPONSE: As per the above suggestion, the inconclusive results for Indian Ocean region are now incorporated in the manuscript. Table S1 (supplementary text) is revised to include the results of initial linear regression analysis for individual parameters from the Indian Ocean region. This analysis is similar to that of Eq. (2) and (3) for Indian + Southern Ocean and Southern Ocean respectively. The values of coefficient of determination (R^2), slope, intercept and p (at 5%) indicate that for this region only the absolute latitude (R^2 = 0.3, p = 0.02) and salinity (R^2 = 0.3, p = 0.02) parameters show statistically significant dependence on the observed sea surface iodide (SSI) concentration. A parameterisation formulated using these parameters is listed in the manuscript Table 2 as Eq. (3a) for Indian Ocean. ANOVA test on dataset for Eq. (3a) provides F ratio of 3.604 and p = 0.053 which indicates that the null hypothesis is accepted as the F ratio is larger than the critical F value from an f-distribution table for (2,15) degrees of freedom. Similarly, for comparison and consistency throughout the text ANOVA test was also performed on datasets of parameterisation given in Eq. (2) and (3).

The results of ANOVA test on these datasets are now discussed in detail in the supplementary text under section 4 between lines L96 – 109. In the manuscript this section is mentioned on lines 248 to 255.

2) Similar statistical analysis is also needed for the different analyses north and south of the polar front. Pearson coefficients for the correlation of observed IO with various parameters divided and combined data set are shown in Fig. 8. These help give some idea of the differences between the correlations on either side of the front, but the picture is incomplete.
Two particular results highlighted in the text are demonstrative: GEOS-Chem modeled IO is significantly correlated with observed IO in the data subsets but not in the complete data set. Fig. 8 shows this also the case for CAM-Chem at ~94% confidence as well. The reason for this, as stated by the authors, is that the variability in both models across the polar front is significantly different than observed. Further, the reader can see this for themselves in Figs. 4 and 10. In contrast, correlations with chl-a are much more difficult to interpret. Most data occupy a limited dynamic range in Fig. 4 and the correlation plots in Fig. 9 indicate individual points may be driving the correlation but this is not clear. In both instances systematic statistical assessment of the data subsets would be helpful.

RESPONSE: The reviewer is right to point that individual data points of chl-*a* are driving the correlation with observed iodine oxide (IO) levels. This point is mentioned in the manuscript on lines 643 – 644. We mentioned that high IO levels were observed in a narrow band where elevated chl-*a* observations were noted close to the Kerguelen Islands at 43º S. Here, the figure was incorrectly marked as Fig. 5 instead of Fig. 4e and this error is now corrected in the manuscript. We agree that systematic assessment of individual regions, and sub-regions would be useful but unfortunately this is not possible due to the low number of datapoints (as pointed out by the reviewer in the first comment).

In addition, I have the following additional two major comments.

3) As the authors state in the abstract their results start from "the first concomitant observations of iodine oxide (IO), O3 in the gas phase, and sea surface iodide concentrations." The choice of "concomitant" implies some intrinsic link between the set of parameters, and theoretically these parameters are expected to correlate via the mechanism outlined by Eqs. 7 and 8. However, the authors ultimately find that the correlations are the opposite of those in the equations as shown in Fig. 8 and discussed in the text. Keeping close to the underlying data these correlations should be shown in full similar to Chl-a in Fig. 9.

RESPONSE: The word ‘concomitant’ was used to highlight the previously established links between sea surface iodide and surface ozone leading to the flux of HOI and I_2 (as evident in Eq. (7) and (8) from literature). This does suggest an intrinsic link between the set of parameters. We agree that the findings in this study are contrary to these expectations and so a correlation of sea surface iodide and ozone concentration with flux of HOI and I_2 (Fig. 7) is included in the manuscript to highlight this point. However, we do not feel that all the correlations which are not significant need to be presented as separate figures as in Fig. 9 as in the case of chl-*a*. All the significant correlations are presented as separate figures and figure 8 shows the parameters which are not significant in a single plot showing the summary.

4) The underlying measurements are contained in four other papers (Chance et al., 2019a,b and Mahajan et al., 2019 a,b) are fundamental to assessing these findings. These are

sufficiently critical to the results presented that I would recommend linking them as companion papers. I cannot locate Chance et al. (2019b) and do not believe it is published. The measurements are described in part in Chance et al. (2019a) nonetheless it is troubling that such critical measurements are neither published nor described more fully. If the measurements are not yet published the description in this paper should be expanded. Notably, MAX-DOAS data (which are published elsewhere) appear in the supplement while the SSI data do not.

RESPONSE: A preprint of the Chance et al. 2019b paper is now available on ESSOAr. The manuscript is currently under review in Frontiers of Marine Science and is cited as Chance et al., 2020 in the manuscript, first appearing on line 128. The sea surface iodide (SSI) data are not included in detail in this manuscript as the Chance 2019 and 2020 papers (cited in the manuscript) have a full description of the dataset – these are both available now.

I have following minor and technical comments.

Line 28: As commented above, "concomitant" here may be misleading in the abstract. While the latter portion of the abstract (L 37-39) makes clear that "Sea-air fluxes ... calculated from the atmospheric ozone and seawater iodide ... failed to adequately explain the detected IO in this region" it does not make clear that the correlations are largely null or even contrary to expectations.

RESPONSE: We are not sure what the reviewer means since the observations of iodide, ozone and IO were indeed made at the same place and time, hence the use of the word concomitant.

Line 58-60: Saiz-Lopez et al. (2006b) included IO condensation onto particles in order to explain particle growth. However, I do not believe there is any claim of direct nucleation by IO. This sentence should be clarified.

RESPONSE: The reviewer is mistaken in this claim – I_2O_2 was considered as 'the condensable unit in the iodine particle nucleation' in the model used in that publication.

Line 73 and 74: Why are these reactions not labeled and numbered?

RESPONSE: These reactions are a part of reaction R1 that show the steps leading to formation of HOI. This is now added and reactions are labelled in the text.

Line 266: The detection limit and precision should match units to be more easily compared.

RESPONSE: Thank you for bringing this to our attention. The units are changed to ppbv for both detection limit and the precision on line number L279.

Line 270-272: Consider simplifying description of wind flagging to inclusion of the forward hemisphere or the like. Presently mildly confusing.

RESPONSE: Added line 284.

Line 302-30: Wind speed is first introduced here but discussed frequently hereafter. What is the wind speed referred to? e.g. is it U10 or some other standard? This is particularly relevant later when comparing with model treatment of wind parameters.

RESPONSE: The wind speed data is referred to the winds arriving at the ship's AWS sensor located at the height of approximately 10 m above the sea. Hence this data is U10 data as per the standard treatment. This information is now included in the manuscript on line number 404.

Line 305 - 307: As is made clear later on line 317, neither of the activation energies determined in MacDonald et al. (2014) is significantly different from zero. While it does not examine the products separately, Magi et al. (1997) does find a significant activation energy for the first I- + O3 reaction. MacDonald et al. noted that the Arrhenius pre-exponential factor in Magi et al. is ten orders of magnitude greater than the diffusion limit to justify assuming an activation energy for the first step of zero. More recent work has also called the rates determined in Magi et al. into question (Moreno et al., 2018), however, the confounding factors (high iodide concentrations and iodide surface activity) cannot fundamentally dispel the observed positive temperature dependence. Notably, the values reported in MacDonald are predicated on an assumption that the activation energy of I- + O3 is zero and it is even more uncertain whether the overall activation energy to produce I2 is negative. The activation energies from MacDonald are better summarized as approximately zero (e.g. Moreno and Baeza-Romero 2019) as the overall temperature dependence remains unresolved.

RESPONSE: We thank the reviewer for pointing out this paper. A short description on the above is now added to the manuscript (Line 333).

Line 401-405: While diurnal variation in O3 can be inferred, its reversal is not apparent in Fig. 5b as referred to.

RESPONSE: We agree with the reviewer that the lack of diurnal variation is not clear in Fig. 5b. An inset is included in this plot to highlight the same and figure is revised.

Line 645 - 646: How do the authors infer that photochemistry is responsible for the differences? This is not obvious to me.

RESPONSE: This has now been changed to 'that either photochemistry or dynamical dilution of the fluxes'.

Line 654 – 655: From Fig. 7 it appears that the p-value for the HOI correlation is 0.04. Given that 5% significance is used as a standard elsewhere in the paper this would indicate that HOI does show significant correlation contrary to this statement.

RESPONSE: Figure 7 shows the correlation of HOI against I^- and not of HOI against IO.

Line 771: VOI not previously introduced.

RESPONSE: This has been edited in the latest version of the manuscript.

Figure 3: The literature calculations are not readily compared with the observations as they are in separate panels. The observations should appear in both panels.

RESPONSE: This has been changed accordingly.

Figure 9: It should be made clear that the IO here is observed as modeled IO is also presented elsewhere. The legends readily blend in with the scattered data and should be made more clearly separate.

RESPONSE: This has now been made clear in the caption.

Table 2: The database location column should be moved left of the equations as it is otherwise unclear in isolation what the differences between Eq. 2, 3, and 5 are. Iodide and nitrate concentrations should be given with consistent (though not necessarily the same) units, i.e. M or mol L-1 but not both.

RESPONSE: We have changed the table as requested. The units of the iodide and nitrate concentrations were chosen to be consistent with the equations from past publications which estimate the iodide using different parameters but have clarified this in the caption.

Table 2 and Supplement: In addition to the expectation of higher R2 values for fitting to the same data set, equations having more degrees of freedom are expected to have better fits. The adjusted R2 values should be used for proper comparison of the overall parameterizations. If this is already the case it should be described as such in the supplement.

RESPONSE: Corrected.

References:

Chance, R., Tinel, L., Sherwen, T., Baker, A., Bell, T., Brindle, J., Campos, M. L. A. M., Croot, P., Ducklow, H., He, P., Hoogakker, B., Hopkins, F. E., Hughes, C., Jickells, T., Loades, D., Macaya, D. A., Mahajan, A. S., Malin, G., Phillips, D. P., Sinha, A. K., Sarkar, A., Roberts, I. J., Roy, R., Song, X., Winklebauer, H. A., Wuttig, K., Yang, M., Zhou, P. and Carpenter, L. J.: Global sea-surface iodide observations, 1967-2018, submitted, doi:10.5285/7e77d6b9-83fb-41e0-e053-6c86abc069d0, 2019a.

Chance, R., Tinel, L., Carpenter, L. J., Sarkar, A., Sinha, A. K., Mahajan, A. S., Chacko, R., Sabu, P., Roy, R., Jickells, T. D., Stevens, D. and Wadley, M.: Surface inorganic iodine speciation in the Indian Ocean and Indian Ocean sector of the Southern Ocean, Manuscr. Prep., 2019b.

MacDonald, S. M., Gómez Martín, J. C., Chance, R., Warriner, S., Saiz-Lopez, A., Carpenter, L. J. and Plane, J. M. C.: A laboratory characterisation of inorganic iodine emissions from the sea surface: Dependence on oceanic variables and parameterisation for global modelling, Atmos. Chem. Phys., 14(11), 5841–5852, doi:10.5194/acp-14-5841-2014, 2014.

Magi, L., Schweitzer, F., Pallares, C., Cherif, S., Mirabel, P. and George, C.: Investigation of the Uptake Rate of Ozone and Methyl Hydroperoxide by Water Surfaces, J. Phys. Chem. A, 101(27), 4943–4949, doi:10.1021/JP970646M, 1997.

Mahajan, A. S., Tinel, L., Hulswar, S., Cuevas, C. A., Wang, S., Ghude, S., Naik, R. K., Mishra, R. K., Sabu, P., Sarkar, A., Anilkumar, N. and Saiz Lopez, A.: Observations of iodine oxide in the Indian Ocean Marine Boundary Layer: a transect from the tropics to the high latitudes, Atmos. Environ. X, 1(January), 100016, doi:10.1016/j.aeaoa.2019.100016, 2019a

Mahajan, A. S., Tinel, L., Sarkar, A., Chance, R., Carpenter, L. J., Hulswar, S., Mali, P., Prakash, S. and Vinayachandran, P. N.: Understanding Iodine Chemistry Over the Northern and Equatorial Indian Ocean, J. Geophys. Res. Atmos., (x), 2018JD029063, doi:10.1029/2018JD029063, 2019b.

Moreno, C. G., Gálvez, O., López-Arza Moreno, V., Espildora-García, E. M. and Baeza-Romero, M. T.: A revisit of the interaction of gaseous ozone with aqueous iodide. Estimating the contributions of the surface and bulk reactions, Phys. Chem. Chem. Phys., 20(43), 27571–27584, doi:10.1039/c8cp04394a, 2018.

Moreno, C. and Baeza-Romero, M. T.: A kinetic model for ozone uptake by solutions and aqueous particles containing I- and Br-, including seawater and sea-salt aerosol, Phys. Chem. Chem. Phys., 21(36), 19835–19856, doi:10.1039/c9cp03430g, 2019

Reviewer #2:

The paper by Swaleha Inamdar et al shows new and simultaneous measurements of iodine oxide (IO), ozone (O3) in the gas phase, and sea surface iodide (I-; SSI) concentrations during the ISOE-9 ship campaign in the Indian Ocean and Southern Ocean in January-February 2017. These measurements are complemented with previously published ship based measurements in the Indian Ocean and Bay of Bengal and with different available parametrizations to compute the iodine (I2) and hypoiodous acid (HOI) fluxes. This study includes important new results which should be publishable after a detailed and careful major revision of the manuscript taking all comments into account.

RESPONSE: We thank the reviewer for the comments and have tried to address the comments below.

General comments:
Earlier studies: The paper misses to refer to other iodine ship-based studies, such as Hepach et al (2016), where iodocarbons, IO, and many different biological parameters were observed and possible biological production mechanisms were discussed. A positive correlation between iodine sources and biology and a biology control is not a new result. This has to be taking into account in the abstract, introduction, discussion, and conclusions of your results. There were earlier ship based measurements of atmospheric IO, I2 and ozone, f.e., in the tropical West Pacific during e.g. the SHIVA campaign (Pfeilsticker et al 2013) and in the Indian Ocean with the OASIS campaign (Krüger et al 2015) which should be mentioned and related to.

RESPONSE: We thank the reviewer for pointing out some of the papers that need to be cited and have included them. The Pfeilsticker et al 2013 and Krüger et al 2015 citations are overviews and do not present any IO data.

Indian Ocean: What about the strong seasonality of the Indian Ocean, physical and biological, which may play an important role for the interpretation of your results? This needs to be included in the introduction and the discussion (see Schott and McCreary 2001; SIBER Report No. 1, 2011). Your paper should go beyond a correlation based only discussion. What are the mechanisms in the Indian Ocean: Any biology, ocean and atmospheric circulation impacts? It would be very interesting to get some more details on the spatial distribution of your observed in-situ quantities compared to satellite and/or global model data, adding maps of e.g. SST, Chl-a, wind, SSI/I2.

RESPONSE: We agree that the seasonality of the Indian Ocean needs to be studied and that these data would be useful to compare with model data and maps of etc. We have already used results from the global models CAM-Chem and use the SST and chl-a from satellites in the discussion. However, we have observations from only during the December-March period and hence cannot speculate more on the seasonality. This is however a study that needs to be done in the future.

Measurement, flux parametrization, and model details, errors and uncertainties: What are the error bars of the measurements especially of SSI and what are the uncertainties of the flux estimates? This needs a careful and detailed discussion in the ms. The observed SSI (Chance et al 2019b under review) study is not available to the readership so that we cannot

find any information about the kind of measurements nor the quality. What was the measurement strategy (day vs night time, how often etc)?

RESPONSE: Full details of the iodide measurements are described in the companion paper Chance et al, 2019b (changed to Chance et al., 2020 in the latest version) that is now available as a preprint on ESSOAr and the manuscript is currently under review in Frontiers of Marine Science. The uncertainties of the iodide method were estimated by repeating each scan 5-6 times, with scan repeatability equal or better than 5%. Calibration was by 2 or 3 standard additions of a KI solution (~10-5or 10-6M). The errors reported here reflect the standard deviation of the repeat scans and the standard error on the intercept and slope of the calibration. Precision was estimated by repeat analysis (n = 6) of selected seawater samples over period of ten days and was found to be lower than 7% relative standard deviation. The following sentence has been added in te manuscript (L189): "*The errors reported here reflect the standard deviation of the repeat scans and the standard error on the intercept and slope of the calibration*." Most samples were diurnal, except for some taken during two time series on the SOE-9 cruise (n=11). The uncertainties on the calculated fluxes have not been estimated here, for two reasons (1) the methods used to calculate fluxes would give very incomparable error types (machine learning vs multiple regression) and (2) the multiple regression proposed in Carpenter et al., 2013 to calculate the iodine fluxes (Eq. 7 and 8) does not mention the associated errors.

Where were the surface water iodide measurements carried out onboard of the ship and when? Does the diurnal cycle play a role? Substantial measurement details are missing and need to be added to understand your ship measurement and study design better.

RESPONSE: Full details of the iodide measurements are described in the companion paper Chance et al, 2019b (changed to Chance et al., 2020 in the latest version) that is now available as a preprint on ESSOAr and manuscript is currently under review in Frontiers of Marine Science. Briefly, surface water samples were obtained manually from the upper 30-70 cm of the sea surface using a metal bucket deployed over the side of the ship upwind near the stern, during the SOE-9 and BoBBLE cruise. Additionally, samples were obtained during using the first depth of CTD rosette casts (estimated at 20m) at 17 (SOE-9) and 8 (SK-333) CTD stations. Manual surface samples were taken (by bucket) at least twice a day along the entire cruise track (except when the ship was stationary for CTD stations). Sampling included two time-series, one at ~40oS, and one in coastal Antarctic waters at ~68oS (around the Polar Front), during which samples were collected at 4 or 6 hour intervals for up to 72 hours. No clear diurnal trends could be discerned, in accordance with previous studies (e.g. Brandão, Ana Claudia M., Angela de Luca Rebello Wagener, and Klaus Wagener, 'Model Experiments on the Diurnal Cycling of Iodine in Seawater', Marine Chemistry, 46.1–2 (1994))

For the observed meteorological data, surface wind is conventionally given as 10 min averages and then there are gusts (instantaneous wind). Currently, you use hourly averages which lead to a smoothing of the average wind speed and thus impact your flux parametrization calculations which are based on a threshold limit of 14 m/s. Next, at which altitude levels onboard of the ship were your wind and others quantities measured? Conventionally 10 m surface wind is used for flux calculations. What did you use and on what are the flux parameterisations based on? The measurement section, data and graphs need a thorough and detailed revision.

RESPONSE: We agree that the wind speeds were averaged as we use hourly averages to calculate the fluxes. However, this is necessary due to the frequency of the other observations.

However, the original data is measured at a high frequency and the winds were measured at U10, which is now mentioned in the manuscript.

Substantial details are also missing for the flux parametrization. How well do the estimated iodine fluxes explain observed surface atmospheric I2 concentrations? What are the largest uncertainties also in contrast to the common bulk parametrizations of air-sea fluxes which have a very high (>50%) uncertainty especially with regard to the role of the wind?

RESPONSE: I_2 was not observed during the cruise as mentioned in the manuscript. A detailed discussion in the flux estimation equations is already presented in (Carpenter et al., 2013) and (MacDonald et al., 2014) and we have made use of those equations to study their applicability to the Indian Ocean, and hence have not expanded beyond the discussion in the methodology section which presents the largest sources of uncertainties. Furthermore, both parametrizations do not give the uncertainties associated with the specific parameters.

What are the main chemistry transport and chemistry climate model uncertainties? What is the role of the meteorology and ocean surface (composition and circulation); is this consistently taken into account in these two models compared to your observations?

RESPONSE: We agree that all models have uncertainties resulting from transport and chemical reactions used. However, a detailed analysis of model uncertainties is beyond the scope of this paper. Model description papers have been cited in the manuscript.

Specific comments:
Line 127-129: Grossmann et al 2013 and others published remote open ocean data. Please rephrase the sentence.

RESPONSE: Changed

Table 1: There are no 2014 measurements listed in the third column although you mention this in the table caption, abstract, introduction etc.

RESPONSE: Corrected

Technical corrections:
Figures and figure captions: The graphs and figure captions are not self-explaining and not presented in a consistent way. The acronyms are mostly not introduced nor are the figures easy to relate to each other, f.e. ozone in Figure 4 and 5 is it the same? What is PF; I assume Polar Front and where is this in Fig 5? All your figures and figure captions need a thorough revision.

RESPONSE: Yes, the data in the figures is the same. The polar front is marked only in the figures which have oceanographic data, as this front has no atmospheric significance for the measured parameters. As suggested by the reviewer, we have checked through the captions and made changes where we felt the details were not sufficient.

References:

Hepach, H. et al., Biogenic halocarbons from the Peruvian upwelling region as tropospheric halogen source, Atmos. Chem. Phys., 16, 12219–12237, 2016.

Krüger K. et al, OASIS-research cruises SO234-2 and SO235 of R/V SONNE in summer 2014 in the tropical Indian: : :, The Indian Ocean Bubble, Issue No., 3, Aug. 2015.

Pfeilsticker K. et al, The SHIVA Western Pacific Campaign in Fall 2011, Malaysian Journal of Science 32 (SCS Sp Issue), 141-148, 2013.

Schott, F.A. and McCreary, J.P., 2001. The monsoon circulation in the Indian Ocean. Progress In Oceanography, 51(1): 1-123.

SIBER Report No.1, Sustained Indian Ocean Biogeochemistry and Ecosystem Research, 2011. Research, 2011.

Reviewer #3

The paper by S. Inamdar is using a large data set of seawater iodide, atmospheric ozone and atmospheric IO concentrations to test the reactive inorganic iodine fluxes calculated from different parameterisations of seawater iodide,. The authors propose new parameterisations of seawater iodide that are specific for given regions of the global ocean, and compared to already established parameterisation for the global ocean. They find that the parameterisation used has little impact on the computed atmospheric IO concentrations. Observed IO concentrations cannot be adequately computed using inorganic iodine fluxes and chemistry. As IO is correlated to Chl-a, the authors suggest a biogenic impact on iodine in the region investigated. The paper is well and clearly written and organized. Iodine fluxes, chemistry and impacts on the atmospheric composition are poorly understood and this study brings a nice input into our understanding. I suggest the paper is published after only minor comments (below) are taken into account.

RESPONSE: We thank the reviewer for the positive comments and have answered the specific comments below and made the corresponding changes in the manuscript.

Minor comments

Section 2.1 iodide parameterisations

Lines 201 to 218 : the argumentation on the need to have regional parameterizations should go in the introduction ?

RESPONSE: Changed.

Line 226 : would be nice to recall why sea surface nitrate concentrations were chosen as a parameter influencing iodide concentrations

RESPONSE: Added.

Section 2.2 ozone measurements
Contaminations on a ship may occur from other sources than the ship's smokestack (such as cooking exhausts, or air conditioning exhausts). Were there any indicator of anthropogenic compounds concentrations available to exclude contaminations?

RESPONSE: Yes, ozone shows very strong effects of the smokestack and these were removed from the observations during data cleaning as mentioned in the manuscript. The cleaning was done using the quick titration of the O_3, which was visually easy to identify, the black carbon observations and the aerosol number observations.

3.Results
3.2 Iodide line 432-433: the end of the sentence is not clear, please reformulate

RESPONSE: Corrected.

3.3 Iodine fluxes line 491: premature to mention discrepancies between modelled and measured IO in this section? Would better fit in the discussion section

RESPONSE: Corrected.

4. Discussion
line 712: concerning the lack of correlation with satellite base Chl-a while in situ Chla oncentrations are correlated to observed IO concentrations. May this be due to geographical differences in what biological species Chl-a represent in these different regions, or may be due to uncertainties in the Chl-a retrieval from satellite, or even also scaling problems. Did the authors try to extract satellite Chl-a where the actual Chl-a in situ measurements were performed to compare one with the other?

RESPONSE: This is correct and the sources of the difference between the satellite and in situ could be many as the reviewer has suggested. The chl-a data from the satellites was extracted from the same location as the in situ observations. This is now added in the manuscript.

Estimation of Reactive Inorganic Iodine Fluxes in the Indian and Southern Ocean Marine Boundary Layer

Swaleha Inamdar[1,2], Liselotte Tinel[3], Rosie Chance[3], Lucy J. Carpenter[3], Prabhakaran Sabu[4], Racheal Chacko[4], Sarat C. Tripathy[4], Anvita U. Kerkar[4], Alok K. Sinha[4], Parli Venkateswaran Bhaskar[4], Amit Sarkar[4,5], Rajdeep Roy[6], ~~Tomas~~ Tomás Sherwen[3,7], Carlos Cuevas[8], Alfonso Saiz-Lopez[8], Kirpa Ram[2] and Anoop S. Mahajan[1]*

[1]Centre for Climate Change Research, Indian Institute of Tropical Meteorology, Ministry of Earth Sciences, Dr Homi Bhabha Road, Pashan, Pune, 411 008, India

[2]Institute of Environment and Sustainable Development, Banaras Hindu University, Varanasi, 221 005, India

[3]Wolfson Atmospheric Chemistry Laboratories, Department of Chemistry, University of York, YO10 5DD, UK

[4]National Centre for Polar and Ocean Research, Goa, 403 804, India

[5]Environment and Life Sciences Research Centre, Kuwait Institute for Scientific Research Centre, Al-Jaheth Street, Shuwaikh, 13109, Kuwait

[6]National Remote Sensing Centre, Department of Space Government of India Balanagar, Hyderabad, 500 037, India

[7]National Centre for Atmospheric Science, University of York, York YO10 5DD, UK

[8]Department of Atmospheric Chemistry and Climate, Institute of Physical Chemistry Rocasolano, CSIC, Madrid, Spain.

* Corresponding author: Anoop S. Mahajan (anoop@tropmet.res.in); phone: +91 20 2590 4526

Abstract

Iodine chemistry has noteworthy impacts on the oxidising capacity of the marine boundary layer (MBL) through the depletion of ozone (O_3) and changes to HO_x (OH/HO_2) and NO_x (NO/NO_2) ratios. Hitherto, studies have shown that the reaction of atmospheric O_3 with surface seawater iodide (I^-) contributes to the flux of iodine species into the MBL mainly as hypoiodous acid (HOI) and molecular iodine (I_2). Here, we present the first concomitant observations of iodine oxide (IO), O_3 in the gas phase, and sea surface iodide concentrations. The results from three field campaigns in the Indian Ocean and the Southern Ocean during 2015~~4~~-2017 are used to compute reactive iodine fluxes to the MBL. Observations of atmospheric IO by MAX-DOAS show active iodine chemistry in this environment, with IO values up to 1 pptv (parts per trillion by volume) below latitudes of 40°S. In order to compute the sea-to-air iodine flux supporting this chemistry, we compare previously established global sea surface iodide parameterisations with new, region-specific parameterisations based on the new iodide observations. This study shows that regional changes in salinity and sea surface temperature play a role in surface seawater iodide estimation. Sea-air fluxes of HOI and I_2, calculated from the atmospheric ozone and seawater iodide concentrations (observed and predicted), failed to adequately explain the detected IO in this region. This discrepancy highlights the need to measure direct fluxes of inorganic and organic iodine species in the marine environment. Amongst other potential drivers of reactive iodine chemistry investigated, chlorophyll-*a* showed a significant correlation with atmospheric IO (R = 0.7 above the 99 % significance level) to the north of the polar front. This correlation might be indicative of a biogenic control on iodine sources in this region.

Keywords: iodine, Southern Ocean, Indian Ocean, marine boundary layer

1. Introduction

Iodine chemistry in the troposphere has gained interest over the last four decades after it was first discovered to cause depletion of tropospheric ozone (O_3) (Chameides and Davis, 1980; Jenkin et al., 1985) and cause changes to the atmospheric oxidation capacity (Davis et al., 1996; Read et al., 2008). Iodine studies in the remote open ocean are important considering its role in tropospheric ozone destruction (Allan et al., 2000), the formation of potential cloud condensation nuclei and impact on cloud radiative properties (McFiggans, 2005; O'Dowd et al., 2002). However, iodine chemistry in the remote open ocean is still not completely understood, with uncertainties remaining around the sources and impacts of atmospheric iodine (Saiz-Lopez et al., 2012; Simpson et al., 2015).

Recent studies of atmospheric iodine chemistry have focused on the detection of iodine oxide (IO) in the marine boundary layer (MBL) as a fingerprint for active iodine chemistry. IO may itself also participate in particle nucleation if present at high concentrations (A. Saiz-Lopez et al., 2006). Iodine containing precursor compounds undergo photo dissociation to produce iodine atoms (I), which rapidly react with ambient ozone, forming IO (Chameides and Davis, 1980). Until recently, fluxes of volatile organic iodine (e.g. CH_3I, CH_2ICl, CH_2I_2) compounds including those originating from marine algae (Saiz-Lopez and Plane, 2004) were considered to be the primary source of iodine in the marine atmosphere (Carpenter, 2003; Vogt et al., 1999). However, the biogenic sources of atmospheric iodine could not account for the levels of IO detected in the tropical MBL (Mahajan et al., 2010a; Read et al., 2008). Currently, inorganic iodine emissions are considered to be the dominant sources contributing to the open ocean boundary layer iodine (Carpenter et al., 2013). A recent study by Koenig et al. (2020) concluded that inorganic iodine sources play major role in comparison to the organic iodine sources in contributing even to the upper troposphere iodine budget. Laboratory investigations revealed that at the ocean surface, iodide (I^-) dissolved in the seawater reacts with the deposited

gas-phase ozone to release hypoiodous acid (HOI) and molecular iodine (I_2) via the following reactions (Carpenter et al., 2013; Gálvez et al., 2016; MacDonald et al., 2014) :

$$I^- + O_3 \rightarrow IOOO^- \quad \text{(R1a)}$$

$$IOOO^- \rightarrow IO^- + O_2 \quad \text{(R1b)}$$

$$IO^- + H^+ \leftrightharpoons HOI \quad \text{(R1c)}$$

$$H^+ + HOI + I^- \rightleftharpoons I_2 + H_2O \quad \text{(R2)}$$

The reaction of sea surface iodide (SSI) with ozone in (R1) is considered a major contributor (600-1000 Tg per year, (Ganzeveld et al., 2009)) to the loss of ozone at the surface ocean, contributing between 20 % (Garland et al., 1980) and 100 % (Chang et al., 2004) of the oceanic ozone dry deposition velocity. Reactions (R1) and (R2) result in the release of reactive iodine (HOI and I_2) to the atmosphere, where they quickly photolyse to yield I atoms, which react with ozone in the gas phase to form IO (Carpenter, 2003; Saiz-Lopez et al., 2012). Carpenter et al. (2013) showed that the reactions (R1) and (R2) could account for about 75 % of the IO levels detected over the tropical Atlantic Ocean. Further studies have shown that including these reactions and the resulting fluxes of HOI and I_2 in atmospheric chemistry models has results in good agreement between observed and modelled iodine levels over the Atlantic and the Pacific Ocean, but not for the Indian and Southern Ocean. For example, the sea-air flux of HOI and I_2 could explain the observed levels of molecular iodine and IO at Cape Verde (Lawler et al., 2014a), and observed IO levels over the eastern Pacific were in reasonable agreement with those modelled from estimated I_2 and HOI fluxes (MacDonald et al., 2014). In contrast, the inorganic iodine fluxes estimated for the Indian Ocean and Indian sector of the Southern Ocean marine boundary layer could not fully explain the observed IO concentrations (Mahajan et al., 2019a, 2019b). Similarly, in the Pacific observations of IO and halocarbons have shown

Field Code Changed
Field Code Changed
Field Code Changed
Field Code Changed

that the contribution of combined iodocarbon fluxes to IO is between 30 to 80% assuming an inorganic iodine lifetime of between 1 and 3 days (Hepach et al., 2016).

Predicted global emissions of iodine compounds show a large sensitivity (~ 50 %) to the SSI field used (Saiz-Lopez et al., 2014; Sherwen et al., 2016c, 2016b); an improved and accurate system for simulating SSI concentration is imperative. Existing global parameterisations discussed in this study follow three different methods for SSI estimation. The first is a linear regression approach against biogeochemical and oceanographic variables (Chance et al., 2014), the second uses an exponential relationship with sea surface temperature as a proxy for SSI (MacDonald et al., 2014), and the third is a recent machine-learning-based model (Sherwen et al., 2019a) that predicts monthly global SSI fields for the present-day. Where such approaches are based on large scale relationships, they may not properly capture smaller scale, regional differences in SSI (as observed for Chance et al., 2014; MacDonald et al., 2014) or underestimate surface iodide concentration (in case of Sherwen et al., 2019).Furthermore, there are large differences in predicted iodide concentrations between these parametrisations in some regions (refer Sect. 3.2). Thus, estimation of seawater iodide based on the existing parameterisations may not always be sufficiently accurate.

At present, there is a paucity of measurements of SSI, and remote sensing techniques cannot detect iodine species in seawater (Chance et al., 2014; Sherwen et al., 2019a). In particular, regions of the Indian Ocean and the Southern Ocean have been under-sampled in terms of iodine observations in the atmosphere and ocean (Chance et al., 2014; Mahajan et al., 2019a, 2019b). It is important to remember that the most widely used parameterisation (MacDonald et al., 2014) is built on a limited observational dataset from the Atlantic and Pacific Ocean completely excluding the Indian Ocean and the Southern Ocean. As they have not been tested in the Indian Ocean, they may not be suitable for accurate estimation of SSI in the distinct and highly variable salinity and temperature regimes of the Indian Ocean region. The

parameterisations presented in Chance et al. (2014), are based on a larger data set including Southern Ocean observations, but still only make use of two data points in the Indian Ocean. Furthermore, the Sherwen et al. (2019) parameterisation uses the updated data set including the new Indian Ocean SSI observations used in this study. Compounding the lack of Indian Ocean SSI observations is the fact that parts and in particular the Arabian Sea and the Bay of Bengal, do not follow the same seasonal trends in salinity (D'Addezio et al., 2015) and sea surface temperature (Dinesh Kumar et al., 2016) as each other on the same latitudinal band and hence the currently used global iodide parameterisations in models i.e. MacDonald et al. (2014) may not be appropriate for these areas. Here we use new SSI observations made as part of this study (described in full in (Chance et al., 2020) and included in Chance et al. (2019~~a~~)) to test whether the existing parameterisations can be directly applied to the Indian Ocean and if regional specific parameterisations are more accurate compared to the former.

Although several measurements of IO have been reported around the globe, including in the open ocean (Alicke et al., 1999; Allan et al., 2000; Frieß et al., 2001; Großmann et al., 2013; Mahajan et al., 2010b, 2010a, 2009; Prados-Roman et al., 2015), the remote open ocean still remains under-sampled. The two documented observations of IO in the Indian Ocean and the Indian sector (Jan-Feb 2015 and December 2015) of the Southern Ocean were interpreted using parameterisations to estimate the SSI concentrations in combination with observed ozone concentrations, to subsequently calculate the resulting inorganic iodine fluxes. This approach suggested that the observed atmospheric IO may not be well correlated with the inorganic fluxes and that biogenic fluxes could play an important role (Mahajan et al., 2019a, 2019b). Here, we present measurements of IO in the MBL of the Indian Ocean and the Southern Ocean during the 9th Indian Southern Ocean Expedition (ISOE-9) conducted in January-February 2017, alongside the first simultaneous SSI observations along the cruise track (Chance et al., 2019). The iodide observations were used to compute the inorganic iodine fluxes to compare

with IO observations along the cruise tracks. Further, observed SSI concentrations are used to compute region-specific parameterisations for SSI concentrations, following the approaches taken by Chance et al. (2014) and MacDonald et al. (2014). The iodide concentrations obtained with these region-specific modified parameterisations are compared to the iodide estimates using their original counterparts and the global machine-learning-based prediction of SSI concentration (Sherwen et al., 2019a). The resulting estimated reactive iodine fluxes (HOI and I_2) are then used to see if the inorganic fluxes can explain the IO loading in the atmospheric MBL.

2. Measurement techniques and methodology

The 9th Indian Southern Ocean Expedition (ISOE-9) was conducted from January to February 2017 in the Southern Ocean and the Indian Ocean sector of the Southern Ocean. The expedition started from Port Louis, Mauritius, and spanned the remote open ocean area till the coast of Antarctica. Observations of IO, SSI and O_3 were made along the cruise track during ISOE-9. For further analysis we also include IO observations from the 2nd International Indian Ocean Expedition (IIOE-2) and the 8th Indian Southern Ocean Expedition (ISOE-8) conducted in the Indian and Southern Ocean region during austral summer of ~~2014~~ 2015 (Mahajan et al., 2019a, 2019b). We also include SSI observations in the northern Indian Ocean from two expeditions namely, the Sagar Kanya-333 cruise (SK-333) and the Bay of Bengal Boundary Layer Experiment (BoBBLE) conducted during June-July and September 2016 respectively (Chance et al., 2020). Table 1 includes details of the expeditions, including the locations, dates of the expeditions and the meridional transect for each expedition. Figure 1a shows a map with the cruise tracks for the five expeditions. Figure 1b shows the seawater iodide sampling locations during ISOE-9, SK-333 and BoBBLE expeditions. The track of the ship during ISOE-9 along with the air mass back trajectories arriving at noon each day is given in the supplementary text Fig. S1. The HYbrid Single-Particle Lagrangian Integrated Trajectory (HYSPLIT) model

(Rolph et al., 2017; Stein et al., 2015) was used to calculate the back trajectories. Similar back trajectory plots and full cruise tracks for ISOE-8 and IIOE-2 are given in Mahajan et al. (2019a, 2019b). During the three expeditions, meteorological parameters of ocean and atmosphere were measured using an on-board automatic weather station and manual observation techniques.

2.1. Sea surface iodide (SSI)

In this section, we focus on developing region-specific parameterisation for SSI estimation by adapting previously established methods. The SSI concentrations obtained from the original and newly developed region-specific parameterisation and SSI model predictions are used for a comparison study, and further to calculate the inorganic iodine emissions.

2.1.1 Observed SSI in the Indian Ocean and the Southern Ocean

Historically, few observations of SSI are available for the Indian Ocean basin with reports of only 3 data points in the open ocean from the Arabian Sea sector of the Indian Ocean (Farrenkopf and Luther, 2002). Two of these values are coastal, and they lack supporting sea surface temperature and salinity data; thus, they have been excluded from this study. However, recent work has led to a large increase in the number of SSI observations available for the Indian Ocean and Southern Ocean (Indian ocean sector) (Chance et al., 2020). Specifically, 111 new observations were made during the 2016 ISOE-9 and 18 during the SK-333 and BoBBLE. During the ISOE-9, SSI measurements in seawater were made concomitant with observations of O_3 and IO in the gas phase for the first time. Observations of SSI made during this expedition used the cathodic stripping voltammetry method with a hanging mercury drop electrode as a working electrode (Campos, 1997; Luther et al., 1988). The errors reported on the concentrations reflect the standard deviation of the repeat scans and the standard error on the intercept and slope of the calibration. The seawater samples were collected during the ISOE-9 at a 3-6-hour interval between 23º S and 70º S. Seawater samples from the SK-333

cruise and BoBBLE were analysed following the same technique for surface iodide concentrations. Iodide data from SK-333 and BoBBLE contributed to 18 additional data points between 10º N and 4º S making a total of 129 new locations (excluding coastal and extremely high values above 400 nM; see (Chance et al., 2020) for details) for observed SSI in the Indian Ocean and Southern Ocean region. This is a major sample size compared to the global 2014 database (n=925) across all the global oceans (Chance et al., 2014), and these data points contribute substantially to the recently updated iodide dataset (Chance et al., 2019) (n=1342). From here onwards, the iodide concentrations obtained from sampling observations will be referred to as measured SSI as opposed to modelled SSI to differentiate between the observed iodide concentrations and those calculated using the parametrisations. All available observations made in the Indian Ocean basin as presented in Chance et al. (2019a) have been included for the development of the region-specific parameterisation presented in this work. Further details about the measurement technique and the observations used can be found in (Chance et al., 2020).

2.1.2 Iodide parametrisations

Due to the sparsity of SSI measurements, different empirical parametrisations have been proposed to estimate SSI concentrations. Parameters like SST and salinity (only for SK-333 and BoBBLE; $R^2 = 0.3$, $P = 0.018$) show a positive correlation with the SSI concentrations. However, a global parameterisation scheme may not capture the specificities of these required for regional studies. The northern Indian Ocean has markedly different sea surface salinity (D'Addezio et al., 2015) and SST (Dinesh Kumar et al., 2016) in its two basins, the Arabian Sea and the Bay of Bengal, that share the same latitude bands separated by the Indian sub-continental landmass. These basins experience the biannually reversing monsoonal winds, which greatly influence their SST and salinity structure. Strong winds in the Arabian Sea associated with the summer monsoon dissipate heat via overturning and turbulent mixing.

Whereas weaker winds in the Bay of Bengal imply high SST due to the formation of stable and shallow surface mixed layer (Shenoi, 2002). The Arabian Sea exhibits much higher salinity compared to the Bay of Bengal due to greater evaporation and lower river runoff (Rao and Sivakumar, 2003). As mentioned earlier, the c~~C~~urrent global SSI parameterisations ~~(MacDonald et al., 2014; Chance et al., 2014)~~ are based almost entirely on observations from the Atlantic, Pacific and Southern ~~(excluding the Indian ocean sector)~~ Oceans, ~~they may not be suitable for accurate estimation of SSI in the distinct and highly variable salinity and temperature regimes of the~~ and have not been tested in the Indian Ocean region.

Here, we aim to create region-specific parameterisations for the Indian and Southern Ocean and conduct a comparison between these and the existing global parameterisations, further discussed in Sect. 4.2. The existing (Eq. (1), Eq. (4), and Eq. (6)) global -and the new region-specific parameterisations are listed in Table 2. Below we describe briefly the modified parameterisations. Details about the original parameterisations can be found in their respective publications (Chance et al., 2014; MacDonald et al., 2014; Sherwen et al., 2019a).

(a) Linear regression analysis was performed, on each parameter, namely, SST, mixed layer depth (MLD), latitude, sea surface nitrate concentration (as it has been suggested that iodate could be reduced by nitrate based enzymes (Chance et al., 2014)), and salinity against the measured SSI concentrations from ISOE-9, SK-333, and BoBBLE campaigns, similar to the Chance et al. (2014) technique, but using in situ SST and salinity observations instead of climatological values. More details on the approach taken can be found in the supplementary text. The combination with the largest R^2 and uniform distribution of residuals from the statistically significant dependent variables, as detailed in Table S1 resulted in Eq. (2) of Table 2. Eq. (2) thus represents a region-specific (the Indian Ocean and the Southern Ocean region abbreviated as Ind. O. + Sou. O. in the figures) variant of the Chance et al. (2014) parameterisation for the estimation of SSI concentrations. Similarly, keeping in mind the

difference in the SST and salinity for the Indian Ocean and the Southern Ocean, another parameterisation was derived only for the Southern Ocean region using the ISOE-9 iodide observations and for the Indian Ocean using the SK-333 and BoBBLE iodide observations, respectively. The parameterisation for the Southern Ocean region using ISOE-9 iodide observations is given in Table 2 as Eq. (3). A similar Indian Ocean parameterisation is formulated and listed in the last row of Table 2 as Eq. (3a). However, this parameterisation is not valid, and it is omitted from analysis in this text due to statistical insignificance inferred from ANOVA test using StatPlus statistical analysis software. In this method, the F ratio from ANOVA analysis is compared with the critical F value from the standard f-distribution table (at 0.05 significance level) to confirm the statistical robustness. Results of ANOVA test on the datasets for Eq. (2), (3) and (3a) is discussed in the supplementary text. ~~included in this text as the linear regression analysis fails to obtain a parametric equation for this region. This may be due to fewer data points (n=18) combined for the Arabian Sea and Bay of Bengal basins.~~

(b) A second method for the estimation of SSI concentration was proposed by MacDonald et al. (2014) that uses the correlation between sea surface iodide and SST. At present, this is the most commonly used parameterisation in global models (Sherwen et al., 2016b, 2016a, 2016c; Stone et al., 2018). Similar to MacDonald et al. (MacDonald et al., 2014) (Table 2, Eq. 4), we derived an Arrhenius-type, region-specific expression using iodide and SST data from ISOE-9, SK-333 and BoBBLE. Figure 2 shows the typical linear dependence of $\ln[I^-]$, for observed SSI in the Indian Ocean and the Southern Ocean, with SST^{-1}, which resulted in the Arrhenius form expression given as Eq. (5) in Table 2.

Figure 3 shows the iodide concentrations for the three campaigns, ISOE-8, IIOE-2 and ISOE-9, calculated using equations (1) to (5), the measured iodide concentrations from ISOE-9, SK-333 and BoBBLE, and the global iodide model predictions obtained from Sherwen et al. (2019) (Table 2.). From here on, region-specific parameterisations developed for SSI concentrations

are referred to as the modified versions of the original parameterisations; Eq. (2) and (3) are called the modified Chance et al. (2014) parameterisation for the Indian Ocean and Southern Ocean region and only the Southern Ocean region, respectively. Eq. (5) is called the modified Macdonald et al. (2014) parameterisation. The machine-learning-based model proposed in Sherwen et al. (2019) is referred to as 'SSI model' results.

2.2. Ozone

Surface ozone was monitored using a US-EPA approved nondispersive photometric UV analyser (Ecotech EC9810B) installed on the ship during the expeditions to detect surface ozone values at a one-minute temporal resolution. A Teflon tube ~ 4 m long fixed towards the front of the ship acted as an inlet for the analyser. The analyser is equipped with a selective ozone scrubber, which was alternatively switched in and out of the measuring stream. The analyser has a lower detection limit of 0.5 ppbv and a precision of ~~0.00~~1 ppb~~m~~v. A 5-micron PTFE filter membrane installed in the sample inlet tube was changed regularly. Zero and span calibration were done every alternate day to ensure accurate O_3 measurements. The ozone data collected was cleaned to remove the data points under the influence of the ship's smokestack by referring to the measured apparent wind direction on the ship. Apparent wind approaching the ship from 0 ° to 90º or 270 ° to 360º (front hemisphere of the ship) was considered free from smokestack emission influence, where 0° or 360º represents the bow of the ship. Ozone data recorded when the ship was stationary showed major smokestack emission influence and was excluded from the data.

2.3. Estimation of inorganic iodine fluxes

In order to estimate the contribution of inorganic iodine chemistry to active iodine chemistry in the atmosphere, the atmospheric fluxes for the main product species, I_2 and HOI, need to be calculated, since direct flux measurements of I_2 and HOI have not been done anywhere in the

world to date. While there are reported observations of marine I_2 emission, they are few in number and mostly from coastal regions (Atkinson et al., 2012; Huang et al., 2010; a Saiz-Lopez et al., 2006) and one observation in the open ocean (Lawler et al., 2014b), although these are all observations of atmospheric concentrations and not of fluxes. As observed SSI is not available for all cruises, we used the following scenarios for SSI to estimate the inorganic iodine fluxes:

(a) Using measured SSI: Observations of sea surface iodide from ISOE-9, SK-333, and BoBBLE.

(b) Using calculated SSI from:

1. Chance et al. (2014) parameterisation Eq. (1)
2. Modified Chance et al. (2014) parameterisation for the Indian Ocean and Southern Ocean (Ind. O. + Sou. O.) region Eq. (2)
3. Modified Chance et al. (2014) parameterisation for the Southern Ocean (Sou. O.) region Eq. (3)
4. MacDonald et al. (2014) parameterisation using SST Eq. (4)
5. Modified MacDonald et al. (2014) parameterisation Eq. (5)
6. Machine-learning-based model prediction (Sherwen et al., 2019a) Eq. (6)

Ozone was measured on all three cruises (ISOE-9, IIOE-2 and ISOE-8). The fluxes for HOI and I_2 were then calculated for all the above scenarios except for the observations from SK-333 and BoBBLE as IO observations were not taken during these cruises. The following algorithm was used for estimating iodine fluxes (Carpenter et al., 2013),

$$flux_{I_2} = \left[O_{3\,(g)}\right] * \left[I^-_{(aq)}\right]^{1.3} * (1.74 \times 10^9 - 6.54 \times 10^8 * \ln(ws)) \quad \text{Eq. (7)}$$

$$flux_{HOI} = \left[O_{3\,(g)}\right] * \left(4.15 \times 10^5 * \frac{\sqrt{\left[I^-_{(aq)}\right]}}{ws} - \frac{20.6}{ws} - 2.36 \times 10^4 * \sqrt{\left[I^-_{(aq)}\right]}\right) \quad \text{Eq. (8)}$$

where, the fluxes are in nmol m^{-2} d^{-1}, [O_3] in nmol mol^{-1} (ppbv), [I^-] in mol dm^{-3} and the wind speed (WS) in m s^{-1}. Carpenter et al. (2013) did not consider the effect of temperature in the interfacial layer of the sea-surface model on activation energies for the reaction R1 (i.e., assumed the temperature dependence for k ($I^- + O_3$) to be zero). Although I_2 and HOI fluxes are expected to increase with the temperature of the interfacial layer, I_2 production has a negative activation energy, as noted by MacDonald et al. (2014). In Carpenter et al. (2013) (specific to the tropical Atlantic), a seawater temperature of 15ºC and air temperature of 20º C were used to calculate Henry's law constants, diffusion constants, and mass transfer velocities. Again assuming the temperature dependence of k($I^- + O_3$) to be zero, but including the temperature-dependence of Henry's law constants, diffusion constants, and mass transfer velocities, the same interfacial layer model predicted effective activation energies for I_2 and HOI emissions of -2 kJ mol^{-1} and 25 kJ mol^{-1} (Macdonald et al. (2014). Using these activation energies, Macdonald et al. (2014) calculated differences in I_2 and HOI fluxes of 3 % and 31-41 %, respectively, at SSTs of 10º C and 30º C compared to the room-temperature parameterisations presented in Carpenter et al. (2013). Experimentally derived activation energies for I_2 and HOI emissions were -7 ± 18 kJ mol-1 and 17 ± 50 kJ mol^{-1} (MacDonald et al., 2014). As HOI represents the larger iodine flux, the higher relative uncertainty in the activation energy should be kept in mind when calculating temperature-dependent emissions. It should be noted that a recent study suggested that the activation energies from MacDonald et al. (2014) are better summarized as approximately zero (e.g. (Moreno and Baeza-Romero, 2019) as the overall temperature dependence remains unresolved.

HOI and I_2 fluxes are also influenced by the wind speed as seen from equations (7) and (8), and the modelled iodine fluxes (HOI and I_2) are highest for high [O_3], high [I^-] and low wind speed. This is explained by the assumption that wind shear drives mixing of the interfacial layer to bulk seawater, reducing the efflux of HOI and I_2 into the atmosphere (Carpenter et al., 2013).

Negative fluxes are obtained from equations (7) and (8) for both HOI and I_2 when the wind speed is higher than 14 m s^{-1} , which is not physically possible and therefore the model output is limited to wind speeds below 14 ms^{-1} (Mahajan et al., 2019a). Iodine fluxes calculated from equations (7) and (8) using SSI concentrations from the scenarios (a) and (b 1-6) are shown in Fig. 4 (c and d).

2.4. Iodine Oxide

2.4.1 Observations

Ship-based measurements of IO were made using the Multi-Axis Differential Optical Absorption Spectroscopy (MAX-DOAS) technique (Hönninger et al., 2004; Platt and Stutz, 2008). The MAX-DOAS was installed at the bow of the ship with a direct line of sight towards the front of the ship to avoid the ship's plume in the detection path of the telescope. The MAX-DOAS was programmed to capture scattered sunlight spectra at every 1 second at set elevation angles of 0, 1, 2, 3, 5, 7, 20, 40, and 90-degrees during daylight hours. Mercury line calibration offset, and dark current spectra were recorded after sunset on each day. Elevation angles outside a range of ±0.2 degree from the set value were eliminated from the 30 minutes averaged spectra for increased accuracy. Figure S2 shows the resultant IO and O_4 differential slant column densities (DSCDs) for ISOE-9 campaign, similar plots are available for ISOE-8 (Mahajan et al., 2019a) and IIOE-2 (Mahajan et al., 2019b). The QDOAS software (Danckaert et al., 2017) was used for DOAS retrieval of IO from the spectra using the optical density fitting analysis method. The spectra were fitted with a 3rd order polynomial using fitting interval of 415 to 440 nm with cross-sections of NO_2 (Vandaele et al., 1998), O_3 (Bogumil et al., 2003), O_4 (Thalman and Volkamer, 2013), H_2O (Rothman et al., 2013), two ring spectra, first as recommended by Chance and Spurr, (1997) and second following Wagner et al.,(2009) and a liquid water spectrum for seawater (Pope and Fry, 1997). To remove the influence of

stratospheric absorption a spectrum corresponding to 90º (zenith) from each scan was used as a reference for the analysis. The raw spectra were analysed to obtain differential slant column densities (DSCDs), and values with a root mean square error (RMS) of greater than 10^{-3} were eliminated. Similarly, DOAS retrieval of O_4 in 350 to 386 nm spectral window was performed, and DSCDs were obtained. The optical density fits for IO and O_4 from ISOE-9 are shown in Fig. S3. The IO DSCDs were then converted to volume mixing ratios using the O_4 slant columns following the previously used "O_4 method" (Mahajan et al., 2012; Prados-Roman et al., 2015; Sinreich et al., 2010; Wagner et al., 2004). Further details of the instrument, retrieval procedure and conversion into mixing ratios can be found in previous works (Mahajan et al., 2019a, 2019b).

2.4.2 Modelled atmospheric IO

We use outputs from two global models for a comparison with the observations conducted during the three cruises. The first model is the GEOS-Chem chemical transport model (version 10-01, 4x5 degrees horizontal resolution, http://www.geos-chem.org,), which includes detailed HOx-NOx-VOC-ozone-halogen-aerosol tropospheric chemistry (Sherwen et al., 2017, 2016b) and is driven by offline meteorology from NASA's Global Modelling and Assimilation Office (http://gmao.gsfc.nasa.gov) forward processing product (GEOS-FP).

The second model is the 3D chemistry-climate model CAM-Chem version 4 (Community Atmospheric Model with Chemistry) https://www2.acom.ucar.edu/gcm/cam-chem), which is included in the CESM framework (Community Earth System Model, CAM-Chem, version 4.0). The model includes a state-of-the-art halogen chemistry scheme (chlorine, bromine and iodine) (Saiz-Lopez and Fernandez, 2016). The current configuration includes an explicit scheme of organic and inorganic iodine emissions and photochemistry. These halogen sources comprise the photochemical breakdown of five very short-lived bromocarbons ($CHBr_3$,

388 CH_2Br_2, CH_2BrCl, $CHBrCl_2$ and $CHBr_2Cl$) naturally emitted by phytoplankton from the
389 oceans (Ordóñez et al., 2012). The model was run in specified dynamic mode (Ordóñez et al.,
390 2012), with a spatial resolution of 1.9º latitude by 2.5º longitude and 26 vertical levels from the
391 surface to up to 40 km.

392 Both models include biotic emissions of four iodocarbons (CH_3I, CH_2ICl, CH_2IBr and CH_2I_2)
393 as described by (Ordóñez et al., 2012) and abiotic oceanic sources of HOI and I_2 based on the
394 Carpenter et al. (2013) and MacDonald et al. (2014) laboratory studies of the oxidation of
395 aqueous iodide by atmospheric ozone at the ocean surface. Both models here use the
396 MacDonald parameterisation expression (Eq. (4), MacDonald et al., 2014) discussed in Section
397 2.1.2 to predict surface iodide used for calculating iodine emissions and the organo-halogen
398 emissions from ~~Ordoñez~~ Ordóñez et al. (2012). IO surface concentrations for the three
399 campaigns (IIOE-2, ISOE-8 and ISOE-9) were extracted from the model runs and used for
400 comparison. Currently, these two global models include reactive iodine chemistry (along with
401 TOMCAT, which includes the tropospheric iodine chemistry (Hossaini et al., 2016)).

402 **3. Results**

403 **3.1 Ozone, Meteorological and Oceanic parameters**

404 The latitudinal distribution of hourly average values of U10 wind speed (WS), O_3, SST, and
405 salinity from all the campaigns are shown in Fig. 5. Winds arriving at the ship, shown in the
406 first panel (Fig. 5a), remained low for most of the duration of all three expeditions with wind
407 speed ranging from 1 m s^{-1} to stronger winds of 24 m s^{-1} on a few days. Even stronger winds
408 (above 30 m s^{-1}) were observed during the ISOE-9 in the region between 64 º and 65º S with
409 the highest wind speed of 32 m s^{-1} at 66º S on the night of 8th February 2017. Ozone mixing
410 ratios, (Fig. 5b) during all three expeditions showed a similar trend exhibiting a large reduction
411 in values in the open ocean environment compared to coastal environments. The back

trajectories (supplementary text) show that for most of the expeditions, air masses arriving at the cruise were from the open ocean environment and did not have any anthropogenic influence for the last five days. This is reflected in the O_3 values, which range between 8 and 20 ppbv in the open ocean but were between 30 and 50 ppbv near the coastal regions, where the air mass back trajectories confirm anthropogenic origins. Close to the Indian sub-continent ozone levels peaked at about 50 ppbv during the ISOE-8. It also showed a distinct diurnal variation with higher ozone values during the daytime due to photochemical production. However, in the open ocean environment, ozone mixing ratios did not show this diurnal variation, and indeed values of ozone dropped during daytime indicating photochemical destruction during both ISOE-8 and ISOE-9 (Fig. 5b).

As already noted, SST is widely used to predict SSI (Eq. 4 and 5). Combined SST data (Fig. 5c) reveal a steady decrease in sea surface temperature from 15º S to 68º S for all the campaigns. During January 2015 (ISOE-8) seawater north of 6º N displays slightly lower SST (~ 3º C) compared to that in December 2015 (IIOE-2). Salinity is also an important parameter for the prediction of SSI (higher coefficient in Eq. 1, 2 and 3). The Southern Ocean region explored during ISOE-8 and ISOE-9 reveals similar salinity values (Fig. 5d) for the austral summer months of 2015~~4~~ and 2016 (January-February). The salinity data shows relatively lower values for ISOE-8 compared to those for IIOE-2 for the region 15º N to 20º S. Despite the inter-annual differences in the northern Indian Ocean region, salinity values of ~ 35 PSU overlap for the IIOE-2 and ISOE-8 in a small window of 7º N to the equator. Below the equator, the salinity values for IIOE-2 increase while for ISOE-8 salinity remains lower than 35 PSU until 20º S. Seawater between 20º S and 44º S has a near-constant salinity of 35 PSU which decreases to ~33.5 PSU after 44º S and remains the same until 65º S after which the salinity begins to drop to 31.5 PSU near 67º S close to Antarctica.

3.2 Sea surface iodide concentration

Latitudinal averages of SSI concentrations estimated from seven scenarios (listed in Sect. 2.3) are shown in Fig. 3. SSI estimates from the IIOE-2 campaign are marked separately to differentiate from the ISOE estimates for the Indian Ocean region. There is a clear difference in the estimated SSI in different scenarios. All the estimates and the model follow a similar pattern showing elevated levels in the tropics as compared to the higher latitudes. SSI estimates from parameterisations (Eq. 1, 3, 4, and 5) show nearly constant values for SSI from 15º N to 25º S, after which a steady decline is noted until 70º S. Thus, the parametrisations based on Eq. 1, 3, 4 and 5 do not capture the decreasing trend observed for iodide around the equator. Eq. 2, which was derived specifically for the Indian Ocean and Southern Ocean region better captures this trend, and also shows a better match with the measured SSI from SK-333 and BoBBLE in the Indian Ocean. Eqn. 6 also predicts lower concentrations around the equator than in the northern Indian Ocean. SSI concentrations estimated using the Chance et al. (2014) parameterisation (Eq. 1) show a small increase in iodide concentrations south of 47º S (polar front), which is not observed in the other parameterisations, but there is some suggestion of an increase in the observations. Eq. 1 also resulted in a large difference (~ 50 nM) of SSI estimates north of 10º N between the IIOE-2 and ISOE-8 cruises; while this difference was lower for the other parameterisations. This difference between the SSI estimates for the IIOE-2 and ISOE-8 cruises is due to the large difference in salinity values for this region (Sect. 4.1). SSI estimates using Eq. 2 shows good agreement with the model prediction of Sherwen et al. (2019), both indicating a decrease in SSI concentrations near the equator during the IIOE-2 and ISOE-8 expeditions. Some high SSI concentrations (up to ~250 nM) were observed around 10º N, these were best replicated by Eqn.3. The highest SSI concentrations estimated using Eq. 3 were 244 nM at 7º N during IIOE-2 and 242 nM at 12º S during ISOE-8. At the equator, Eq. 2 performs better in predicting the SSI concentrations with a difference of ~75 nM compared to the observations. SSI estimates from Eq. 4, i.e. MacDonald et al. (2014) parameterisation, were

462 lower than the measured iodide concentrations and all other parameterisation, including the
463 model (Eq. 7) predictions. Overall, all modified parameterisations (Eq. 2, 3 and 5) estimate
464 higher SSI compared to the original parameterisation (Eq. 1 and 4), with the exception of the
465 region south of 20º S, where Eq. 3 predicts lower SSI than Eq. 1. The modified MacDonald
466 parameterisation (Eq. 5) estimated iodide concentrations to be greater by 50 nM for the entire
467 dataset in comparison to the existing MacDonald parameterisation given by Eq. 4. For Eq. 5,
468 the uncertainty in the iodide concentration from the 95 % prediction band is ~15 % of the
469 predicted value.

470 **3.3 Iodine fluxes**

471 Figure 4 shows the latitudinal variation in IO mixing ratios, inorganic iodine emissions (HOI
472 and I_2), chl-*a* and ozone mixing ratios for the entire dataset comprising of the three campaigns.
473 All the panels in Fig. 4 are plots of daily averaged values during each expedition, except for
474 the HOI and I_2 fluxes; these are latitudinal averages from each campaign. Emissions calculated
475 using the measured SSI concentrations (represented by filled spheres in Fig. 4 c & d) from
476 ISOE-9 correspond to the data points of the measured SSI concentration. Oceanic inorganic
477 iodine emission fluxes of HOI and I_2 were estimated using the Carpenter et al. (2013)
478 parameterisation given in Eq. (7) and (8) limited to wind speeds below 14 m s^{-1}. Thus, the
479 fluxes estimated from the measured SSI concentrations were reduced to 56 points (out of 111
480 measured SSI data points). The seven different datasets of iodide concentrations (listed in Sect.
481 2.3) have been used for estimation of HOI and I_2 fluxes. For the entire dataset, the highest
482 fluxes were obtained when using the SSI concentrations from the modified Chance et al. (2014)
483 parameterisation (Eq. 3), derived from measured SSI from the Southern Ocean region, i.e.
484 during ISOE-9. The second highest fluxes were estimated using SSI from Eq. 2, obtained from
485 measured SSI from the Indian Ocean and Southern Ocean. Comparatively lower iodine
486 emissions were estimated using SSI concentration from MacDonald et al. (2014)

parameterisation (Eq. 4). The estimated inorganic iodine fluxes in the Southern Ocean region (30º S and below) are much lower compared to the Indian Ocean (Fig. 5), driven by the higher estimated SSI in the latter. Maximum inorganic emissions are predicted in the tropical region, specifically, north of the equator. HOI is the dominant reactive iodine precursor species for the entire dataset, with calculated flux values 20 times higher than those for I_2. Emissions estimated using SSI from Eq. (3), resulted in a peak HOI flux of 1.5×10^9 molecules cm^{-2} s^{-1} at 9º N during ISOE-8. The lowest HOI flux of 1.7×10^6 molecules cm^{-2} s^{-1} was obtained at 61º S during ISOE-9. For the same latitudes (9º N and 61º S), a maximum I_2 flux of 7.0×10^7 molecules cm^{-2} s^{-1} and a minimum of 1.3×10^5 molecules cm^{-2} s^{-1} were estimated, respectively. Flux estimates from Eq. 2 are slightly lower, with a maximum HOI flux of 1.3×10^9 and a minimum of 5.8×10^5 molecules cm^{-2} s^{-1} and maximum I_2 flux of 5.2×10^7 with minimum of 8.3×10^4 molecules cm^{-2} s^{-1} at the same latitudes. The estimated HOI and I_2 emissions are notably lower (by ~50 %) during IIOE-2 to the north of 5ºS compared to emissions from ISOE-8. Between 5º S and 20º S, the emissions from IIOE-2 and ISOE-8 are similar. Fluxes estimated using measured SSI concentrations for the ISOE-9 campaign (20º S to 70º S) show no strong latitudinal trend for both HOI and I_2 emissions. The maximum calculated HOI flux was 5.8×10^8 molecules cm^{-2} s^{-1} at 68º S and the minimum was 1.1×10^7 molecules cm^{-2} s^{-1} at 33º S. Similarly, I_2 fluxes estimated from measured SSI concentrations peaked at 1.5×10^7 molecules cm^{-2} s^{-1} at 32º S with a minimum of 3.5×10^5 molecules cm^{-2} s^{-1} at 67º S. Inorganic iodine emissions estimated using model predictions for SSI concentrations from Sherwen et al. (2019) match well with the fluxes estimated using the iodide parametrisation tools. Despite the differences in SSI concentrations from existing and region-specific parameterisations, all result in similar values for iodine fluxes ~~and so SSI cannot explain discrepancies in the observed and modelled IO levels in this region~~.

3.4 Iodine oxide

3.4.1 Observations

IO was detected above the instrument detection limit (2.1 - 3.5 × 10^{13} molec. cm^{-2} i.e. 0.4 – 0.7 pptv) in all three campaigns. The expeditions covered a track from the Indian Ocean to the Antarctic coast in the Southern Ocean and showed lower IO DSCDs in the tropics compared to the Southern Ocean, with a peak of about 3 x 10^{13} molec. cm^{-2} at 40° S. Figure 4a shows daily averaged IO mixing ratios for all the three cruises combined. IO mixing ratios of up to 1 pptv were observed in the region 50° - 55° S and slightly higher values of IO mixing ratios were observed in the region below 65° S close to the Antarctic coast. North of the polar front region, the maximum IO average mixing ratio of ~1 pptv was observed at 40° S. The highest values of IO were observed close to the Antarctic coast, with up to 1.5 pptv measured during ISOE-9 and similar values are reported for the ISOE-8 expedition south of the polar front (Mahajan et al., 2019a). The IO mixing ratios in the Southern Ocean region for ISOE-9 ranged between 0.1 and a maximum of 1.57 (± 0.37) pptv observed on 18 Feb 2017 at 50° S on a clear sky day. This maximum value was observed only on one day, and preceded by foggy and misty days, later followed by overcast for several days evidencing the role of photochemistry in IO production from its precursor gases.

3.4.2 Modelled IO

Based on the current understanding of iodine chemistry, regional and global models consider inorganic fluxes of iodine (HOI and I_2) as major contributors of iodine in the marine boundary layer. It is important to verify if the models using the existing parameterisation for these source gases can replicate observations of IO in the region of study. Thus, we have included model IO output from GEOS-Chem and CAM-Chem, both of which use the SST based MacDonald et al. (2014) parameterisation for SSI (Fig. 4b). The surface IO output from GEOS-Chem predicts the highest levels of IO up to 1.7 pptv to the north of the equator at 11° N for the time period of the IIOE-2 campaign. For the same latitudes, the model suggests lower IO levels, of less than 0.5 pptv, during the ISOE-8 campaign. Conversely, south of the equator to 10° S, the

model predicts higher IO levels during the ISOE-8 and lower IO values during the IIOE-2, in agreement with the observations. Below 10º S, IO predictions for both campaigns match well until 20º S, which was the latitudinal limit for the IIOE-2 campaign. To the south of 20º S, modelled IO levels remained below 1 pptv and exhibited a decreasing trend to the south of the polar front, in disagreement with IO observations. At locations between 40º S and 43º S, GEOS-Chem underestimates the observed IO levels by 50 %. These locations are close to the Kerguelen Islands, and high IO values were observed here only during the ISOE-8. These locations have been omitted in the correlation study between modelled and observed IO as they could be impacted by coastal or upwelling emissions, which are not well prescribed in the models.

The CAM-Chem IO surface output suggests consistently higher levels of IO during IIOE-2 compared to the ISOE-8 for the same latitudinal band (Fig. 4b). Contrary to the observations, the CAM-Chem model suggests that IO levels during the IIOE-2 are up to 1 pptv higher than the ISOE-8 campaign near 7º S latitude. The model also shows elevated IO levels of 2.7 pptv at 7.9º N during the IIOE-2 campaign, which does not match the observations during the IIOE-2 or the ISOE-8 for that region. IO levels below 1.5 pptv (11º N to 20º S) are indicated for the ISOE-8 campaign. In addition, the region between 0º and 1.5º S has similar IO levels for the IIOE-2 and ISOE-8 campaigns. The model predicts lower IO levels for the south Indian Ocean and the Southern Ocean (less than 1 pptv) with decreasing IO to the south of the polar front. However, at 43º S, the model suggests higher IO (2.4 pptv) during the ISOE-9, which matches the increase in observed IO for that region during the ISOE-8 expedition, with this region being close to the Kerguelen Islands Both models show consistently higher absolute concentrations overall compared to the observations north of the polar front.

4. Discussion

561 **4.1 Seawater iodide**

562 To improve the estimation of SSI in the study region, previously established parameterisations
563 (Eq. 1 and 4) were modified to obtain a region-specific parameterisation for SSI concentrations.
564 SSI estimated using these modified parameterisations were less sensitive to seasonal salinity
565 and SST changes for the north Indian Ocean basin compared to the existing parameterisation
566 (Fig 3). Figure 6 shows the correlations of all the calculated SSI concentrations with the
567 observations. The SSI estimates from Eq. 1 to 6 correlate positively (significantly) to the
568 measured SSI concentrations (observations) from ISOE-9 (Fig. 6). Out of the six
569 parameterisation tools compared in this study, as expected, SSI from Eq. (2) i.e. the modified
570 Chance equations for the Indian Ocean and the Southern Ocean showed the best correlation
571 with the measured SSI because they were created using datasets from these campaigns (Fig. 6
572 and Table 2). Although the region-specific parameterisations were expected to match with the
573 observations they are based on, there was a notable difference between predictions and
574 observations when this approach was applied only to Indian Ocean SSI measurements from
575 SK-333 and BoBBLE (R^2 = 0.5 for Indian Ocean parameterisation, analysis not shown). This
576 could be attributed to the lack of SSI measurements in this region (n=18), and it highlights the
577 fact that there may be not only seasonally but regionally varying complexities in SSI which
578 should be considered when estimating SSI. All parameterisation methods used for SSI
579 estimations show that SSI concentrations are directly proportional to seawater salinity (listed
580 in Sect. 2.3). It is evident from Fig. 5d and Fig. 3a that to the north of the equator, the
581 parameterisations (Eq. 1 to 5) show lower SSI concentrations in regions with lower salinity (up
582 to 5º N during ISOE-8 – filled symbols Fig. 3) and higher SSI concentrations in regions with
583 comparatively higher salinity (during IIOE-2 – unfilled symbols Fig. 3). Only the modelled
584 SSI concentrations using Eq. 6 (Fig. 3a, data in purple) reveal an inversely proportional
585 relationship for salinity and SSI concentration in this region. The Sherwen et al. (2019)

parametrisation (Eq. 6) produces lower SSI concentrations in high salinity Arabian Sea waters during IIOE-2 (Fig. 3a) north of 5º N, compared to the low salinity Bay of Bengal waters during ISOE-8 which contradicts all the other parameterisation (Eq. 1 to 5). Further, the SSI concentrations obtained from Sherwen et al. (2019) reverse their trend to the south of 6º N, with higher concentrations during IIOE-2 and lower during ISOE-8. It should be noted that only a few observations of SSI exist in this region to confirm this trend. Further discussion on the relationship between salinity and other biogeochemical variables with SSI concentrations at a global and regional scale can be found elsewhere (Chance et al., 2014, 2019).

SSI estimates considering only SST as a proxy for iodide concentration (Eq. 4), reveal positive correlations with measured SSI concentration ($R = 0.86$, $P<0.001$, $n = 129$; Fig. 6d). The modified MacDonald parameterisation (Eq. 5) also correlates positively to the measured SSI concentration but has a slightly lower coefficient of correlation ($R = 0.83$, $P<0.001$, $n = 129$; Fig. 6e). When using the SST as a proxy for SSI, a large intercept was obtained for the SSI values, evidencing the discrepancy in absolute value between this parametrisation and the observations. Eq. (5) resulted in a lower intercept, approximately half of that for Eq. (4), and a lower absolute slope value of |-3763±218| compared to the |-9134±613| of Eq. (4) given in MacDonald et al. (2014). The lower absolute slope value for Eq. (5) implies that the SSI concentrations for this region were less sensitive to the changes in SST compared to that in Eq. (4).

Despite the lower R-value, the SSI estimates from Eq. 5 in Fig. 3 are closer to the measured SSI concentration than the estimates from Eq. 2 and 3 for the region from 25º S to 70º S. However, north of 25º S, the SSI estimates from Eq. 3 and Eq. 5 differ by ~40 %. Both SST based parameterisation (Eq. 4 and 5) did not show the observed latitudinal variation in the SSI concentrations near the equator. Linear regression of SSI with SST for only the Indian Ocean region revealed that there was no correlation between the two ($R^2 = 0.07$, $P = 0.3$, $n = 18$). The

SSI in this region only showed dependence on the salinity and latitude, correlations with the other parameters were not significant. This highlights that SST may not be a very good proxy for SSI in the Indian Ocean, especially near the equator. This is explored further in Chance et al. (~~Chance et al.,~~ 2020). The original Chance et al. (2014) parameterisation displays higher sensitivity to seasonal salinity changes compared to the existing and modified parameterisation in the Indian Ocean region (Sect. 3.3). However, this method predicted increasing iodide concentration to the south of the polar front (47º S), which is not supported by observations in this region (Fig. 3). In conclusion, considering the correlation with measured SSI concentration and dependence on seawater salinity, the region-specific modified Chance parameterisation (Eq. 2) is a suitable method to estimate SSI concentration for the Indian Ocean and Southern Ocean region. The modelled SSI estimates by Sherwen et al. (2019) capture SSI trend close to equator better than other existing schemes but it fails to replicate higher SSI observations at locations 8º N, 40º S and to the south of 65º S close to the Antarctic coast (Fig. 3).

4.2 Atmospheric iodine

Combined IO observations from IIOE-2, ISOE-8, and ISOE-9 (Fig. 4a) show that the Indian Ocean region has comparatively less IO in its MBL than the Southern Ocean region. IO remained below 1 pptv up to 40º S and reached a maximum IO of 1.6 pptv south of the polar front. Modelled surface IO output from GEOS-Chem and from CAM-Chem using the Macdonald et al. (2014) parameterisation (Fig. 4b) do not match the observations of IO, although they generally show good agreement with each other. The models show similar spatial patterns across the entire dataset, except for two periods of very high IO levels predicted by CAM-Chem (Fig. 4b). As well as structural differences between CAM-Chem and GEOS-Chem, there are many halogen specific differences in rate constants, heterogeneous parameters, cross-sections and photolysis of species (e.g. higher iodine oxides) which could explain differences in predicted gas-phase IO. Considering the generally lower wind speeds

and higher ozone concentrations seen in IIOE-2 versus SOE-8 and SOE-9, the calculated fluxes are higher and therefore more sensitive to assumptions, such as minimum wind speeds provided to the Carpenter et al. (2013) parameterisation. GEOS-Chem uses a minimum wind speed of 5 m s^{-1}; however, CAM-Chem uses a minimum wind speed of 3 m s^{-1}.

Both models suggest higher than observed IO levels in the Indian Ocean region but under-predict IO for the Southern Ocean region. The highest detected IO levels, both in the Southern Ocean and in a narrow band around 43º S, were not reflected in the model predictions. We note these occurred in regions of elevated chl-*a* values (Fig. 4e~~5~~) close to the Kerguelen Islands.~~,~~ ~~and that~~ Mahajan et al. (2019a) also reported positive correlations for IO with chl-*a* for the Indian Ocean region, above the polar front for a subset of the dataset (ISOE-8). Calculated fluxes of HOI and I_2 (Fig. 4c and d) fail to directly explain trends in the detected IO levels for the entire dataset, regardless of the method used to estimate SSI. Maximum levels of HOI and I_2 predicted to the north of 5º N correspond to rather low levels of IO (< 0.5 pptv) in this region. However, this has been attributed to NO_x titration of IO (Mahajan et al., 2019b). The models, however, do not capture this iodine titration by NO_x as seen in the observations; even though the reactions of IO with NOx are included (Ordóñez et al., 2012). Similarly, for the region south of the polar front, the calculated iodine fluxes remain low in the region of the maximum detected IO concentrations during the ISOE-8 and ISOE-9 campaigns. Iodine fluxes estimated for the Indian Ocean region (15º N to 5º N) during IIOE-2 and ISOE-8 show large differences with much higher values during ISOE-8. However, the modelled IO is in fact higher for IIOE-2 than during ISOE-8 (5º-15ºN). Considering that the models do not reflect the fluxes, this indicates that either photochemistry or dynamical dilution of the fluxes led to this difference in the model. Additionally, the elevated levels of IO predicted in the models suggest that CAM-Chem and GEOS-Chem overestimate the impact of iodine chemistry in the northern Indian Ocean.

In Fig. 7, correlations of iodine fluxes estimated using the measured SSI concentrations (Eq. 2) show that fluxes of HOI correlate positively with tropospheric ozone ($R = 0.56$, $P<0.001$) and negatively to wind speed ($R = -0.62$, $P<0.001$) and I_2 fluxes correlate positively with SSI concentration ($R = 0.56$, $P = P<0.001$) and ozone ($R = 0.59$, $P<0.001$) and negatively to wind speed ($R = -0.4$, $P<0.001$). This indicates that although there is positive correlation of I_2 with SSI, the dominant inorganic iodine flux i.e. HOI does not show significant correlation with SSI concentration, although the flux equation includes an iodide term (Eq. 8). We analysed the correlation of daily averaged observed IO during the three campaigns with daily averaged values of oceanic parameters (SST, chl-*a*, salinity, SSI concentration), meteorological parameters (wind speed, ozone) and calculated inorganic iodine fluxes. We divided the combined dataset from three campaigns into two regional subsets for the north (Fig. 8a) and south (Fig. 8b) of the polar front (47º S). The correlation for SSI concentrations is included for all the seven methods for SSI estimation listed in Sect. 2.3. The fluxes of HOI and I_2 obtained using the seven different datasets for SSI are included and listed in Fig. 8 in the same order as the SSI concentration (labelled 1 to 7). IO model output from GEOS-Chem (labelled 8) and CAM-Chem (labelled 9) is included for the correlation analysis, along with chl-*a* data from observations during ISOE-8 and ISOE-9 and satellite dataset obtained from MODIS Aqua (Oceancolor, NASA-GSFC, 2017).

For the entire dataset (Fig. 8c), only wind speed shows a statistically significant, positive correlation with observed IO above the 99 % confidence limit ($R = 0.4$, $P<0.001$, $n = 115$). A similar positive correlation with wind speed was found in the subset of data south of the polar front (Fig. 8b) ($R = 0.49$, $P = 0.01$, $n = 48$), with observations north of the polar front showing a weaker positive correlation ($R = 0.27$, $P = 0.08$, $n = 67$). Mahajan et al. (2012) showed that no correlation existed between IO and wind speed over the eastern Pacific Ocean, contrary to the results in this study. Current estimation methods for iodine emissions have a negative

686 dependence on wind speed (Eq. 7 and 8). A positive correlation of IO with wind speed could
687 suggest that increased vertical mixing enables emission of HOI and I_2, and/or other iodine
688 gases, thus enhancing IO production in the MBL. However, the interfacial model still over
689 predicts IO concentrations at low wind speeds due to over prediction of HOI and I_2 emission
690 (MacDonald et al., 2014). The apparently contradictory results from different studies call for
691 more observations of IO in the MBL over a range of wind speeds.

692 Salinity and SST show a weak negative correlation with atmospheric IO for the entire dataset
693 and for the north of the polar front region. This indicates that even if the physical parameters
694 are significant for the initial parametrisation for SSI and inorganic flux estimation, there is no
695 direct and significant correlation of these parameters with the atmospheric IO. However, south
696 of the polar front, SST correlates positively above the 99 % limit ($R = 0.52$, $P = 0.01$, $n = 48$)
697 and salinity correlates positively above the 95 % limit ($R = 0.44$, $P = 0.03$, $n = 48$). Ozone
698 correlates negatively with IO above 95 % limit ($R = -0.4$, $P = 0.046$, $n = 47$), which could
699 indicate catalytic destruction of tropospheric ozone through atmospheric iodine cycling in the
700 south of the polar front. This highlights that although these physical parameters may be
701 required for iodine fluxes, IO levels may only be weakly related to them.

702 The calculated SSI concentrations and the HOI and I_2 fluxes calculated using these SSIs all
703 show a significant negative correlation with the observed IO concentrations above the 95 %
704 confidence limit for the entire dataset (except for the HOI flux estimated from the MacDonald
705 et al. (2014) parameterisation, which shows no significant correlation). The positive correlation
706 of the observed IO with wind speed is a potential driver for the negative correlation of observed
707 IO with the calculated HOI and I_2 fluxes, which decrease with wind speed.

708 Measured iodide levels (labelled 4) and the I_2 and HOI fluxes calculated from them (also
709 labelled 4) show no correlation with the observed IO levels across the entire dataset, although

iodide shows a significant positive correlation (R = 0.55, P = 0.04, n = 32) for IO measured south of the polar front. Mahajan et al. (2019a) pointed out that SST negatively correlated with IO for the ISOE-8 campaign, contradicting the previous results for observations in the Pacific Ocean (Großmann et al., 2013; Mahajan et al., 2012). Here, SST shows a significant positive correlation with observed IO (R = 0.52, P = 0.006, n = 48) south of the polar front above the 99 % confidence limit, but there is no correlation north of the polar front and only a weak negative correlation using the combined dataset from the three campaigns (R = -0.18, P = 0.13, n = 119).

Despite the above-mentioned point regarding the increase in observed IO levels in regions of elevated chl-*a*, there is only a weak and negative correlation of IO with chl-*a* (both from observations and satellite data) south of the polar front. However, there is a strong positive relationship north of the polar front (R = 0.696, P = 2.3×10^{-4}, n = 29). In fact, for the region north of the polar front, chl-*a* shows a significant positive correlation with observed IO above the 99 % confidence limit (P < 0.001). The GEOS-Chem and CAM-Chem output also shows a significant positive correlation (Fig. 8)which may result from the dependency of organic iodine species on oceanic chl-*a* in both GEOS-Chem and CAM-Chem. Figure 8 shows a large difference in correlation values for chl-*a* data obtained from observations and satellite (MODIS Aqua, NASA, GSFC; https://oceancolor.gsfc.nasa.gov; extracted for the same locations as the in situ data). In situ, observed chl-*a* showed an improved correlation with IO compared to those with satellite chl-*a*. Figure 9 shows linear fits for chl-*a* from in situ observations and satellite against IO for the entire dataset and north of polar front subset. For the entire dataset, correlation of chl-*a* with IO from both observations and satellite data is not significant. Chl-*a* from in situ observations positively correlates with IO (R = 0.15, P = 0.32) while chl-*a* from satellite data correlates negatively (R = -0.13, P = 0.26). Correlations of chl-*a* with IO improves for the north of polar front for chl-*a* from observations (R = 0.696, P = 0.0002), but chl-*a* from

satellite data shows a statistically insignificant correlation with IO (R = 0.08, P = 0.57). The discrepancies in chl-*a* from observations and satellite data will make it difficult to identify links between the organic parameter and atmospheric IO and expand this to a global scale. It should be noted that one study in the Pacific has shown that the contribution of combined biogenic iodocarbon fluxes to IO does not explain the observed IO (Hepach et al., 2016).

Despite the observed negative relationship of IO with wind speed noted above, note that the GEOS-Chem IO model output (which is dependent on the calculated HOI and I_2 fluxes) shows a significant positive correlation with observed IO above the 99 % confidence limit for data south (R = 0.78, P = P<0.001, n = 48) and north (R = 0.69, P = P<0.001, n = 68) of the polar front, although there is no correlation across the entire dataset. Note that the model underestimates IO values by 1 pptv south of the polar front and generally overestimates IO, by ~1.5 pptv, north of the polar front (Fig. 4). A linear fit for observed IO against modelled IO for north and south of the polar front (Fig. 10) shows significant positive correlation of GEOS-Chem output with observed IO, but with very different slopes north of the polar front (where the models overestimate IO) and south of the polar front (where the models underestimate IO). Hence, even though the correlations are good in the individual regions, the model does not accurately reproduce the observed absolute concentrations.

5. Conclusions

In this study, region-specific parameterisation tools were devised for sea surface iodide (SSI) estimation following previous SSI estimation methods from Chance et al. (2014) and MacDonald et al. (2014). New observations of SSI from ISOE-9, SK-333 and BoBBLE (Indian and the Southern Ocean) were used to create region-specific SSI parameterisations. An average difference of up to 40 % in SSI concentration was observed among the existing

parameterisations (Eq. 1, 4, and 6) and the difference was 21 % for the region-specific ones (Eq. 2, 3, and 5). Comparison of estimated SSI concentrations from various parameterisations with observed SSI and sensitivity to seasonal salinity changes showed that the modified Chance parameterisation (Eq. 2) was most suitable relative to the SST based parameterisation (Eq. 5) for SSI estimation in the Indian Ocean and Southern Ocean region. Since the existing global parameterisation schemes (Eq. 1 and 3) fail to match measured SSI in this region, it highlights the need to conduct more observations of SSI in the Indian Ocean and Southern Ocean region to fully understand and estimate the impact of seasonally varying, region-specific parameters (like salinity, reversing winds patterns) influencing the seawater iodide concentration in this region. Alternatively, a region-specific parameterisation scheme may be included in the global models for better representation of seawater iodine chemistry in the Indian and Southern Ocean region. Modelled estimates from Sherwen et al. (2019) also captured SSI well, although some high concentrations in the northern Indian Ocean region were not captured. SSI estimation from SST alone under-predicts SSI for the Indian Ocean, and so is not considered to be suitable for SSI estimation in the Indian Ocean region. Although, improving SSI concentration in models for the Indian Ocean and Southern Ocean region may improve the estimation of seawater iodine chemistry, it does not translate to estimating the atmospheric iodine chemistry in this region. An accurate estimation of inorganic iodine fluxes (HOI and I_2) is hence necessary to explain observed levels of IO in the remote open ocean marine boundary layer. However, these first concomitant observations of SSI and IO show that these inorganic fluxes, estimated in this study, fail to explain detected IO levels for the entire dataset. No significant correlation was seen between the SSI from different parameterisation techniques or estimated inorganic iodine fluxes with observed IO levels. Fluxes estimated using iodide from different parameterisation and measured iodide did not show large variation in values and followed a similar latitudinal trend. This is indicative that the inorganic iodine flux parameterisation is not highly sensitive

784 to the SSI parameterisation. Predicted inorganic iodine fluxes did not explain iodine chemistry,
785 as indicated by IO levels, in the atmosphere above the Indian and Southern Ocean (Indian
786 Ocean sector). Chl-*a* shows a positive correlation with IO for the north of the polar front region,
787 suggesting that biologically emitted species could also play a role in addition to ozone and
788 iodide derived inorganic emissions of HOI and I_2. Finally, model predictions of IO
789 underestimate IO levels for the Southern Ocean region but overestimate IO in the Indian Ocean.
790 Models greatly underestimate IO in regions with higher chl-*a* concentration which could be
791 indicative of organic species playing a role (close to the Kerguelen Islands, refer Sect. 3.4.2).
792 This study suggests that the fluxes of iodine in the MBL are more complex than considered at
793 present and further studies are necessary in order to parameterise accurate inorganic and
794 organic fluxes that can be used in models. Using seawater iodide measurements and
795 calculations from different parameterisations did not alter the inorganic iodide flux estimate
796 greatly. Direct observations of HOI and I_2, alongside volatile organic iodine measurements in
797 the MBL are necessary in order to reduce the uncertainty in the impacts of iodine chemistry.

798 **6. Author contributions:**

799 ASM conceptualised the research plan and methodology. SI did the data curation, analysis, and
800 writing of the original draft. LT and RC did the iodide measurements provided unpublished
801 iodide data from ISOE-9, SK-333 and BoBBLE. PS and RCo provided salinity data for ISOE-
802 9. SCT and AUK provided chl-a data for ISOE-9. AKS and PVB provided chl-a data for SK-
803 333. AS and RR provided chl-a data from BoBBLE. CC and ASL did the CAM-Chem model
804 run for ISOE-9 and IIOE-2. TS did the GEOS-Chem model run for ISOE-9, IIOE-2 and ISOE-
805 8.

806 **7. Acknowledgements**

807 The authors thank the Ministry of Earth Sciences for funding the expeditions and IITM for
808 providing research fellowship to Swaleha Inamdar. We would particularly like to thank the
809 ISOE and IIOE-2 teams for their tireless contribution in manually recording and compiling
810 atmospheric and oceanic observations during the expedition. We express gratitude towards the
811 officers, crew and scientist on board RV S. A. Agulhas and RV Sagar Kanya ships for their
812 support. LJC, LT, RC and TS thank the UK NERC (NE/N009983/1) for funding.

813 **8. References**

814 Alicke, B., Hebestreit, K., Stutz, J., Platt, U., 1999. Iodine oxide in the marine boundary
815 layer. Nature 397, 572–573. https://doi.org/10.1038/17508

816 Allan, B., McFiggans, G., Plane, J.M.C., Coe, H., 2000. Observations of iodine monoxide in
817 the remote marine boundary layer. J. Geophys. … 105, 14363–14369.

818 Atkinson, H.M., Huang, R.-J., Chance, R., Roscoe, H.K., Hughes, C., Davison, B.,
819 Schönhardt, A., Mahajan, A.S., Saiz-Lopez, A., Hoffmann, T., Liss, P.S., 2012. Iodine
820 emissions from the sea ice of the Weddell Sea. Atmos. Chem. Phys. 12, 11229–11244.
821 https://doi.org/10.5194/acp-12-11229-2012

822 Bogumil, K., Orphal, J., Homann, T., Voigt, S., Spietz, P., Fleischmann, O.C., Vogel, A.,
823 Hartmann, M., Kromminga, H., Bovensmann, H., Frerick, J., Burrows, J.P., 2003.
824 Measurements of molecular absorption spectra with the SCIAMACHY pre-flight model:
825 Instrument characterization and reference data for atmospheric remote-sensing in the
826 230-2380 nm region. J. Photochem. Photobiol. A Chem. 157, 167–184.
827 https://doi.org/10.1016/S1010-6030(03)00062-5

828 Campos, M.L.A.M., 1997. New approach to evaluating dissolved iodine speciation in natural
829 waters using cathodic stripping voltammetry and a storage study for preserving iodine
830 species. Mar. Chem. 57, 107–117. https://doi.org/10.1016/S0304-4203(96)00093-X

831 Carpenter, L.J., 2003. Iodine in the marine boundary layer. Chem. Rev. 103, 4953–4962.
832 https://doi.org/Doi 10.1021/Cr0206465

833 Carpenter, L.J., MacDonald, S.M., Shaw, M.D., Kumar, R., Saunders, R.W., Parthipan, R.,
834 Wilson, J., Plane, J.M.C., 2013. Atmospheric iodine levels influenced by sea surface
835 emissions of inorganic iodine. Nat. Geosci. 6, 108–111.
836 https://doi.org/10.1038/ngeo1687

837 Chameides, W.L., Davis, D.D., 1980. Iodine: Its possible role in tropospheric
838 photochemistry. J. Geophys. Res. 85, 7383–7398.
839 https://doi.org/10.1029/JC085iC12p07383

840 Chance, R., Baker, A.R., Carpenter, L., Jickells, T.D., 2014. The distribution of iodide at the
841 sea surface. Environ. Sci. Process. Impacts 16, 1841–1859.
842 https://doi.org/10.1039/C4EM00139G

843 Chance, R., Liselotte, T., Sarkar, A., Sinha, A.K., Mahajan, A.S., Chacko, R., Sabu, P., Roy,
844 R., Jickells, T.D., Stevens, D., Wadley, M., Carpenter, L.J., 2020. Surface Inorganic
845 Iodine Speciation in the Indian and Southern Oceans from 12o N to 70o S. Earth Sp. Sci.
846 Open Arch. 36. https://doi.org/10.1002/essoar.10502894.1

847 Chance, R., Tinel, L., Sherwen, T., Baker, A., Bell, T., Brindle, J., Campos, M.L.A.M.,
848 Croot, P., Ducklow, H., He, P., Hoogakker, B., Hopkins, F.E., Hughes, C., Jickells, T.,
849 Loades, D., Macaya, D.A., Mahajan, A.S., Malin, G., Phillips, D.P., Sinha, A.K., Sarkar,
850 A., Roberts, I.J., Roy, R., Song, X., Winklebauer, H.A., Wuttig, K., Yang, M., Zhou, P.,
851 Carpenter, L.J., 2019. Global sea-surface iodide observations, 1967-2018. Nat. Sci. Data
852 6. https://doi.org/doi.org/10.1038/s41597-019-0288-y

853 Chance, K. V., Spurr, R.J.D., 1997. Ring effect studies: Rayleigh scattering, including
854 molecular parameters for rotational Raman scattering, and the Fraunhofer spectrum.

855 Appl. Opt. 36, 5224–5230. https://doi.org/10.1364/AO.36.005224

856 Chang, W., Heikes, B.G., Lee, M., 2004. Ozone deposition to the sea surface: chemical
857 enhancement and wind speed dependence. Atmos. Environ. 38, 1053–1059.
858 https://doi.org/10.1016/j.atmosenv.2003.10.050

859 D'Addezio, J.M., Subrahmanyam, B., Nyadjro, E.S., Murty, V.S.N., 2015. Seasonal
860 Variability of Salinity and Salt Transport in the Northern Indian Ocean. J. Phys.
861 Oceanogr. 45, 1947–1966. https://doi.org/10.1175/JPO-D-14-0210.1

862 Danckaert, T., Fayt, C., Van Roozendael, M., 2017. QDOAS 3.2, Software User Manual.

863 Davis, D., Crawford, J., Liu, S., McKeen, S., Bandy, A., Thornton, D., Rowland, F.S., Blake,
864 D., 1996. Potential impact of iodine on tropospheric levels of ozone and other critical
865 oxidants. J. Geophys. Res. - Atmos. 101, 2135–2147.

866 Dinesh Kumar, P.K., Paul, Y.S., Muraleedharan, K.R., Murty, V.S.N., Preenu, P.N., 2016.
867 Comparison of long-term variability of Sea Surface Temperature in the Arabian Sea and
868 Bay of Bengal. Reg. Stud. Mar. Sci. 3, 67–75.
869 https://doi.org/10.1016/j.rsma.2015.05.004

870 Farrenkopf, A.M., Luther, G.W., 2002. Iodine chemistry reflects productivity and
871 denitrification in the Arabian Sea : evidence for flux of dissolved species from sediments
872 of western India into the OMZ. Deep Sea Res. Part II 49, 2303–2318.

873 Frieß, U., Wagner, T., Pundt, I., Pfeilsticker, K., Platt, U., Friefi, U., 2001. Spectroscopic
874 Measurements of Tropospheric Iodine Oxide at Neumayer Station, Antarctica. Geophys.
875 Res. Lett. 28, 1941–1944.

876 Gálvez, Ó., Teresa Baeza-Romero, M., Sanz, M., Pacios, L.F., 2016. A theoretical study on
877 the reaction of ozone with aqueous iodide. Phys. Chem. Chem. Phys. 18, 7651–7660.

878 https://doi.org/10.1039/c5cp06440f

879 Ganzeveld, L., Helmig, D., Fairall, C.W., Hare, J., Pozzer, A., 2009. Atmosphere-ocean
880 ozone exchange: A global modeling study of biogeochemical, atmospheric, and
881 waterside turbulence dependencies. Global Biogeochem. Cycles 23, 1–16.
882 https://doi.org/10.1029/2008GB003301

883 Garland, J.A., Elzerman, A.W., Penkett, S.A., Penket, S.A., 1980. The Mechanism for Dry
884 Deposition of Ozone to Seawater Surfaces. J. Geophys. Res. 85, 7488–7492.

885 Großmann, K., Frieß, U., Peters, E., Wittrock, F., Lampel, J., Yilmaz, S., Tschritter, J.,
886 Sommariva, R., von Glasow, R., Quack, B., Krüger, K., Pfeilsticker, K., Platt, U., 2013.
887 Iodine monoxide in the Western Pacific marine boundary layer. Atmos. Chem. Phys. 13,
888 3363–3378. https://doi.org/10.5194/acp-13-3363-2013

889 Hepach, H., Quack, B., Tegtmeier, S., Engel, A., Bracher, A., Fuhlbrügge, S., Galgani, L.,
890 Atlas, E.L., Lampel, J., Frieß, U., Krüger, K., 2016. Biogenic halocarbons from the
891 Peruvian upwelling region as tropospheric halogen source. Atmos. Chem. Phys. 16,
892 12219–12237. https://doi.org/10.5194/acp-16-12219-2016

893 Hönninger, G., von Friedeburg, C., Platt, U., 2004. Multi Axis Differential Optical
894 Absorption Spectroscopy (MAX-DOAS). Atmos. Chem. Phys. Discuss. 3, 5595–5658.
895 https://doi.org/10.5194/acpd-3-5595-2003

896 Hossaini, R., Chipperfield, M.P., Saiz-Lopez, A., Fernandez, R., Monks, S., Feng, W.,
897 Brauer, P., Von Glasow, R., 2016. A global model of tropospheric chlorine chemistry:
898 Organic versus inorganic sources and impact on methane oxidation. J. Geophys. Res.
899 121, 14,271-14,297. https://doi.org/10.1002/2016JD025756

900 Huang, R.J., Seitz, K., Neary, T., O'Dowd, C.D., Platt, U., Hoffmann, T., 2010. Observations

of high concentrations of I2 and IO in coastal air supporting iodine-oxide driven coastal new particle formation. Geophys. Res. Lett. 37, 1–5. https://doi.org/10.1029/2009GL041467

Jenkin, M.E., Cox, R.A., Candeland, D.E., Division, M.S., 1985. Photochemical aspects of tropospheric iodine behaviour. J. Atmos. Chem. 2, 359–375. https://doi.org/10.1007/BF00130748

Koenig, T.K., Baidar, S., Campuzano-Jost, P., Cuevas, C.A., Dix, B., Fernandez, R.P., Guo, H., Hall, S.R., Kinnison, D., Nault, B.A., Ullmann, K., Jimenez, J.L., Saiz-Lopez, A., Volkamer, R., 2020. Quantitative detection of iodine in the stratosphere. Proc. Natl. Acad. Sci. 201916828. https://doi.org/10.1073/pnas.1916828117

Lawler, M.J., Mahajan, A.S., Saiz-Lopez, A., Saltzman, E.S., 2014a. Observations of I2at a remote marine site. Atmos. Chem. Phys. https://doi.org/10.5194/acp-14-2669-2014

Lawler, M.J., Mahajan, A.S., Saiz-Lopez, A., Saltzman, E.S., 2014b. Observations of I2 at a remote marine site. Atmos. Chem. Phys. 14, 2669–2678. https://doi.org/10.5194/acp-14-2669-2014

Luther, G.W., Swartz, C.B., Ullman, W.J., 1988. Direct determination of iodide in seawater by cathodic stripping square wave voltammetry. Anal. Chem. 60, 1721–1724. https://doi.org/10.1021/ac00168a017

MacDonald, S.M., Gómez Martín, J.C., Chance, R., Warriner, S., Saiz-Lopez, A., Carpenter, L.J., Plane, J.M.C., 2014. A laboratory characterisation of inorganic iodine emissions from the sea surface: dependence on oceanic variables and parameterisation for global modelling. Atmos. Chem. Phys. 14, 5841–5852. https://doi.org/10.5194/acp-14-5841-2014

924 Mahajan, A.S., Gómez Martín, J.C., Hay, T.D., Royer, S.-J., Yvon-Lewis, S.A., Liu, Y., Hu,
925 L., Prados-Román, C., Ordóñez, C., Plane, J.M.C., Saiz-Lopez, A., 2012. Latitudinal
926 distribution of reactive iodine in the Eastern Pacific and its link to open ocean sources.
927 Atmos. Chem. Phys. 12, 11609–11617. https://doi.org/10.5194/acp-12-11609-2012

928 Mahajan, A.S., Oetjen, H., Saiz-Lopez, A., Lee, J.D., McFiggans, G.B., Plane, J.M.C., 2009.
929 Reactive iodine species in a semi-polluted environment. Geophys. Res. Lett. 36.

930 Mahajan, A.S., Plane, J.M.C., Oetjen, H., Mendes, L.M., Saunders, R.W., Saiz-Lopez, A.,
931 Jones, C.E., Carpenter, L.J., McFiggans, G.B., 2010a. Measurement and modelling of
932 tropospheric reactive halogen species over the tropical Atlantic Ocean. Atmos. Chem.
933 Phys. 10, 4611–4624.

934 Mahajan, A.S., Shaw, M., Oetjen, H., Hornsby, K.E., Carpenter, L.J., Kaleschke, L., Tian-
935 Kunze, X., Lee, J.D., Moller, S.J., Edwards, P.M., Commane, R., Ingham, T., Heard,
936 D.E., Plane, J.M.C., 2010b. Evidence of reactive iodine chemistry in the Arctic
937 boundary layer. J. Geophys. Res. 115. https://doi.org/dx.doi.org/10.1029/2009JD013665

938 Mahajan, A.S., Tinel, L., Hulswar, S., Cuevas, C.A., Wang, S., Ghude, S., Naik, R.K.,
939 Mishra, R.K., Sabu, P., Sarkar, A., Anilkumar, N., Saiz Lopez, A., 2019a. Observations
940 of iodine oxide in the Indian Ocean Marine Boundary Layer: a transect from the tropics
941 to the high latitudes. Atmos. Environ. X. https://doi.org/10.1016/j.aeaoa.2019.100016

942 Mahajan, A.S., Tinel, L., Sarkar, A., Chance, R., Carpenter, L.J., Hulswar, S., Mali, P.,
943 Prakash, S., Vinayachandran, P.N., 2019b. Understanding Iodine Chemistry over the
944 Northern and Equatorial Indian Ocean. J. Geophys. Res. Atmos. 0–3.
945 https://doi.org/10.1029/2018JD029063

946 McFiggans, G.B., 2005. Marine aerosols and iodine emissions. Nature 433, E13–E13.

947 Monterey, G., Levitus, S., 1997. Seasonal Variability of Mixed Layer Depth for the World
948 Ocean. U.S. Government Printing Office, Washington, D.C.

949 Moreno, C., Baeza-Romero, M.T., 2019. A kinetic model for ozone uptake by solutions and
950 aqueous particles containing I− and Br−, including seawater and sea-salt aerosol. Phys.
951 Chem. Chem. Phys. 21, 19835–19856. https://doi.org/10.1039/C9CP03430G

952 O'Dowd, C.D., Jimenez, J.L., Bahreini, R., Flagan, R.C., Seinfeld, J.H., Hämeri, K., Pirjola,
953 L., Kulmala, M., Gerard Jennings, S., Hoffmann, T., Hameri, K., Jennings, S.G., 2002.
954 Marine aerosol formation from biogenic iodine emissions. Nature 417, 632–636.
955 https://doi.org/10.1038/nature00773.1.2.3.4.5.6.7.8.9.10.

956 Ordóñez, C., Lamarque, J.-F., Tilmes, S., Kinnison, D.E., Atlas, E.L., Blake, D.R., Sousa
957 Santos, G., Brasseur, G., Saiz-Lopez, A., 2012. Bromine and iodine chemistry in a
958 global chemistry-climate model: description and evaluation of very short-lived oceanic
959 sources. Atmos. Chem. Phys. 12, 1423–1447. https://doi.org/10.5194/acp-12-1423-2012

960 Platt, U., Stutz, J., 2008. Differential Absorption Spectroscopy, in: Differential Optical
961 Absorption Spectroscopy. Springer, Berlin, Heidelberg, pp. 135–174.
962 https://doi.org/10.1007/978-3-540-75776-4_6

963 Pope, R.M., Fry, E.S., 1997. Absorption spectrum (380–700 nm) ofpure water . II .
964 Integrating cavity measurements. Appl. Opt. 36, 8710–8723.

965 Prados-Roman, C., Cuevas, C. a., Hay, T., Fernandez, R.P., Mahajan, A.S., Royer, S.-J., Galí,
966 M., Simó, R., Dachs, J., Großmann, K., Kinnison, D.E., Lamarque, J.-F., Saiz-Lopez,
967 A., 2015. Iodine oxide in the global marine boundary layer. Atmos. Chem. Phys. 15,
968 583–593. https://doi.org/10.5194/acp-15-583-2015

969 Rao, R.R., Sivakumar, R., 2003. Seasonal variability of sea surface salinity and salt budget of

970 the mixed layer of the north Indian Ocean. J. Geophys. Res. 108, 3009.
971 https://doi.org/10.1029/2001JC000907

972 Read, K.A., Mahajan, A.S., Carpenter, L.J., Evans, M.J., Faria, B.V.E., Heard, D.E.,
973 Hopkins, J.R., Lee, J.D., Moller, S.J., Lewis, A.C., Mendes, L.M., McQuaid, J.B.,
974 Oetjen, H., Saiz-Lopez, A., Pilling, M.J., Plane, J.M.C., 2008. Extensive halogen-
975 mediated ozone destruction over the tropical Atlantic Ocean. Nature 453, 1232–1235.
976 https://doi.org/10.1038/nature07035

977 Rolph, G., Stein, A., Stunder, B., 2017. Real-time Environmental Applications and Display
978 sYstem: READY. Environ. Model. Softw. 95, 210–228.
979 https://doi.org/10.1016/j.envsoft.2017.06.025

980 Rothman, L.S., Gordon, I.E., Babikov, Y., Barbe, A., Chris Benner, D., Bernath, P.F., Birk,
981 M., Bizzocchi, L., Boudon, V., Brown, L.R., Campargue, A., Chance, K., Cohen, E.A.,
982 Coudert, L.H., Devi, V.M., Drouin, B.J., Fayt, A., Flaud, J.M., Gamache, R.R.,
983 Harrison, J.J., Hartmann, J.M., Hill, C., Hodges, J.T., Jacquemart, D., Jolly, A.,
984 Lamouroux, J., Le Roy, R.J., Li, G., Long, D.A., Lyulin, O.M., Mackie, C.J., Massie,
985 S.T., Mikhailenko, S., Müller, H.S.P., Naumenko, O. V., Nikitin, A. V., Orphal, J.,
986 Perevalov, V., Perrin, A., Polovtseva, E.R., Richard, C., Smith, M.A.H., Starikova, E.,
987 Sung, K., Tashkun, S., Tennyson, J., Toon, G.C., Tyuterev, V.G., Wagner, G., 2013. The
988 HITRAN2012 molecular spectroscopic database. J. Quant. Spectrosc. Radiat. Transf.
989 130, 4–50. https://doi.org/10.1016/j.jqsrt.2013.07.002

990 Saiz-Lopez, a, Shillito, J. a, Coe, H., Plane, J.M.C., 2006. Measurements and modelling of I_2,
991 IO, OIO, BrO and NO_3 in the mid-latitude marine boundary layer. Atmos. Chem. Phys.
992 6, 1513–1528. https://doi.org/10.5194/acp-6-1513-2006

993 Saiz-Lopez, A., Fernandez, R.P., 2016. On the formation of tropical rings of atomic halogens:

994 Causes and implications. Geophys. Res. Lett. 43, 1–8.
995 https://doi.org/10.1002/2015GL067608

996 Saiz-Lopez, A., Fernandez, R.P., Ordóñez, C., Kinnison, D.E., Gómez Martín, J.C.,
997 Lamarque, J.-F., Tilmes, S., 2014. Iodine chemistry in the troposphere and its effect on
998 ozone. Atmos. Chem. Phys. 14, 13119–13143. https://doi.org/10.5194/acp-14-13119-
999 2014

1000 Saiz-Lopez, A., Plane, J.M.C., 2004. Novel iodine chemistry in the marine boundary layer.
1001 Geophys. Res. Lett. 31, L04112. https://doi.org/10.1029/2003GL019215

1002 Saiz-Lopez, A., Plane, J.M.C., Baker, A.R., Carpenter, L.J., von Glasow, R., Martín, J.C.G.,
1003 McFiggans, G.B., Saunders, R.W., Gómez Martín, J.C., 2012. Atmospheric Chemistry
1004 of Iodine. Chem. Rev. 112, 1773–1804. https://doi.org/10.1021/cr200029u

1005 Saiz-Lopez, A., Plane, J.M.C., McFiggans, G.B., Williams, P.I., Ball, S.M., Bitter, M., Jones,
1006 R.L., Hongwei, C., Hoffmann, T., 2006. Modelling molecular iodine emissions in a
1007 coastal marine environment: the link to new particle formation. Atmos. Chem. Phys. 6,
1008 883–895.

1009 Shenoi, S.S.C., 2002. Differences in heat budgets of the near-surface Arabian Sea and Bay of
1010 Bengal: Implications for the summer monsoon. J. Geophys. Res. 107, 3052.
1011 https://doi.org/10.1029/2000JC000679

1012 Sherwen, T., Chance, R.J., Tinel, L., Ellis, D., Evans, M.J., Carpenter, L.J., 2019a. A
1013 machine-learning-based global sea-surface iodide distribution. Earth Syst. Sci. Data 11,
1014 1239–1262. https://doi.org/10.5194/essd-11-1239-2019

1015 Sherwen, T., Chance, R.J., Tinel, L., Ellis, D., Evans, M.J., Carpenter, L.J., 2019b. A
1016 machine learning based global sea-surface iodide distribution. Earth Syst. Sci. Data

1017 Discuss. 1–40. https://doi.org/10.5194/essd-2019-40

1018 Sherwen, T., Evans, M.J., Sommariva, R., Hollis, L.D.J., Ball, S.M., Monks, P.S., Reed, C.,
1019 Carpenter, L.J., Lee, J.D., Forster, G., Bandy, B., Reeves, C.E., Bloss, W.J., 2017.
1020 Effects of halogens on European air-quality. Faraday Discuss. 200, 75–100.
1021 https://doi.org/10.1039/C7FD00026J

1022 Sherwen, T., Evans, M.J., Spracklen, D. V., Carpenter, L.J., Chance, R., Baker, A.R.,
1023 Schmidt, J.A., Breider, T.J., 2016a. Global modeling of tropospheric iodine aerosol.
1024 Geophys. Res. Lett. 43, 10012–10019. https://doi.org/10.1002/2016GL070062

1025 Sherwen, T., Evans, M.J.J., Carpenter, L.J.J., Andrews, S.J.J., Lidster, R.T.T., Dix, B.,
1026 Koenig, T.K.K., Volkamer, R., Saiz-Lopez, A., Prados-Roman, C., Mahajan, A.S.S.,
1027 Ordóñez, C., Sinreich, R., Ortega, I., Volkamer, R., Saiz-Lopez, A., Prados-Roman, C.,
1028 Mahajan, A.S.S., Ordóñez, C., 2016b. Iodine's impact on tropospheric oxidants: a global
1029 model study in GEOS-Chem. Atmos. Chem. Phys. 16, 1161–1186.
1030 https://doi.org/10.5194/acp-16-1161-2016

1031 Sherwen, T., Schmidt, J.A., Evans, M.J., Carpenter, L.J., Großmann, K., Eastham, S.D.,
1032 Jacob, D.J., Dix, B., Koenig, T.K., Sinreich, R., Ortega, I., Volkamer, R., Saiz-Lopez,
1033 A., Prados-Roman, C., Mahajan, A.S., Ordóñez, C., 2016c. Global impacts of
1034 tropospheric halogens (Cl, Br, I) on oxidants and composition in GEOS-Chem. Atmos.
1035 Chem. Phys. 16, 12239–12271. https://doi.org/10.5194/acp-2016-424

1036 Simpson, W.R., Brown, S.S., Saiz-Lopez, A., Thornton, J. a., Glasow, R. Von, 2015.
1037 Tropospheric Halogen Chemistry: Sources, Cycling, and Impacts. Chem. Rev.
1038 150312153236002. https://doi.org/10.1021/cr5006638

1039 Sinreich, R., Coburn, S., Dix, B., Volkamer, R., 2010. Ship-based detection of glyoxal over
1040 the remote tropical Pacific Ocean. Atmos. Chem. Phys. 10, 11359–11371.

https://doi.org/10.5194/acp-10-11359-2010

Stein, A.F., Draxler, R.R., Rolph, G.D., Stunder, B.J.B., Cohen, M.D., Ngan, F., 2015. Noaa's hysplit atmospheric transport and dispersion modeling system. Bull. Am. Meteorol. Soc. 96, 2059–2077. https://doi.org/10.1175/BAMS-D-14-00110.1

Stone, D., Sherwen, T., Evans, M.J., Vaughan, S., Ingham, T., Whalley, L.K., Edwards, P.M., Read, K.A., Lee, J.D., Moller, S.J., Carpenter, L.J., Lewis, A.C., Heard, D.E., 2018. Impacts of bromine and iodine chemistry on tropospheric OH and HO2: Comparing observations with box and global model perspectives. Atmos. Chem. Phys. https://doi.org/10.5194/acp-18-3541-2018

Thalman, R., Volkamer, R.A., 2013. Temperature Dependent Absorption Cross-Sections of O2-O2 collision pairs between 340 and 630 nm and at atmospherically relevant pressure. Phys. Chem. Chem. Phys. 15, 15371–15381. https://doi.org/10.1039/C3CP50968K

Vandaele, A.C., Hermans, C., Simon, P.C., Carleer, M., Colin, R., Fally, S., Mérienne, M.F., Jenouvrier, A., Coquart, B., 1998. Measurements of the NO_2 absorption cross-section from 42000 cm^{-1} to 10000 cm^{-1} (238–1000 nm) at 220 K and 294 K. J. Quant. Spectrosc. Radiat. Transf. 59, 171–184. https://doi.org/10.1016/S0022-4073(97)00168-4

Vogt, R., Sander, R., von Glasow, R., Crutzen, P.J., 1999. Iodine Chemistry and its Role in Halogen Activation and Ozone Loss in the Marine Boundary Layer: A Model Study. J. Atmos. Chem. 32, 375–395.

Wagner, T., Beirle, S., Deutschmann, T., 2009. Three-dimensional simulation of the Ring effect in observations of scattered sun light using Monte Carlo radiative transfer models. Atmos. Meas. Tech. 2, 113–124. https://doi.org/10.5194/amt-2-113-2009

Wagner, T., Dix, B., Friedeburg, C. V., Frieß, U., Sanghavi, S., Sinreich, R., Platt, U., 2004.

MAX-DOAS O4 measurements: A new technique to derive information on atmospheric aerosols - Principles and information content. J. Geophys. Res. D Atmos. 109, 1–19. https://doi.org/10.1029/2004JD004904

9. Figures

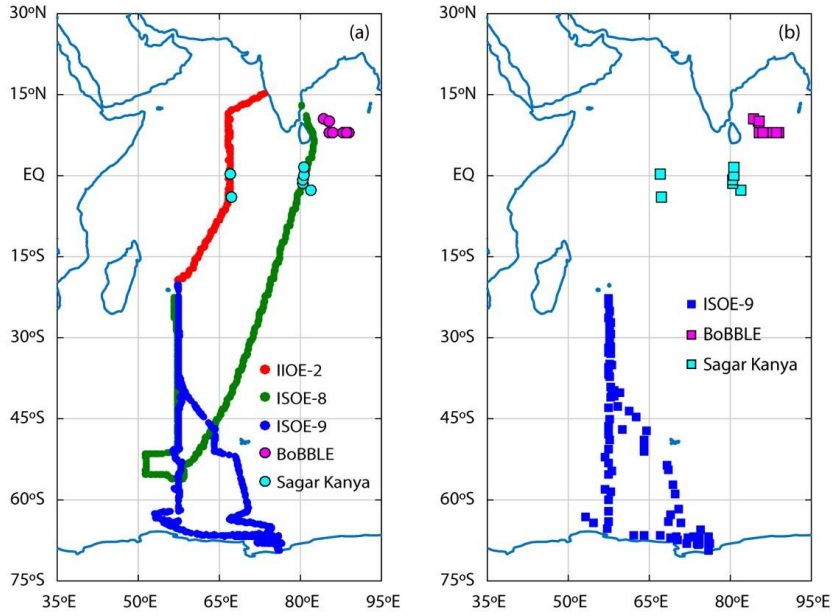

Figure 1: Map of the Indian Ocean and the Southern Ocean (a) with cruise tracks for campaigns conducted during the austral summer of 2014-2016. Green circles indicate the cruise track for ISOE-8, red circles show the cruise track for IIOE-2, and blue circles indicate the cruise track for ISOE-9. Magenta and cyan circles indicate sample locations for the BoBBLE and SK-333 expeditions respectively. (b) boxes represent 129 seawater iodide sampling locations from 3 expeditions following the colour code in (a).

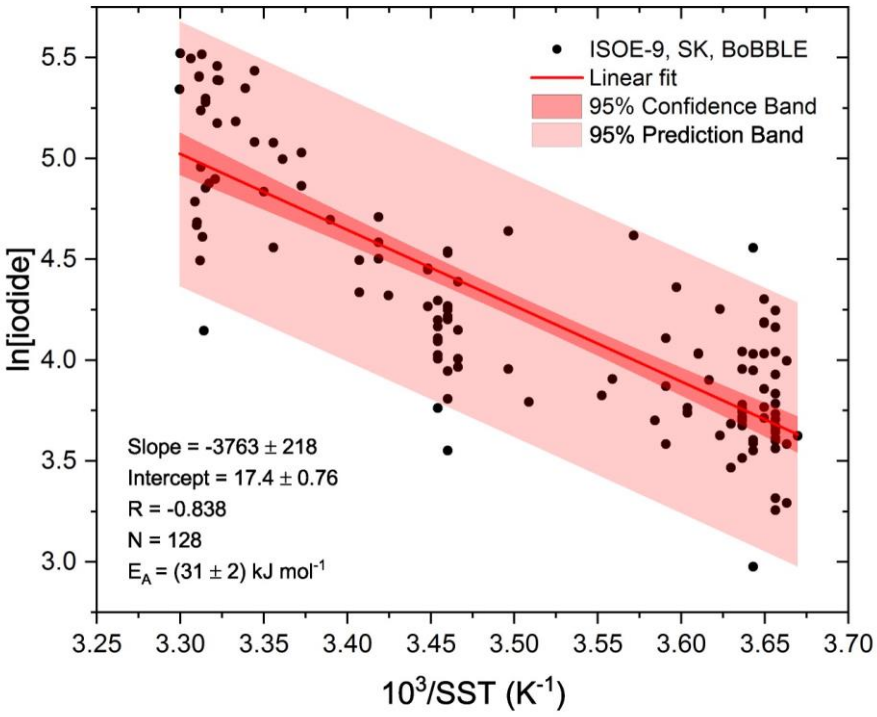

Figure 2: Arrhenius form plot of sea surface iodide concentrations against SST from all available seawater iodide field observations in the Indian Ocean and Southern Ocean. The red line represents a linear fit., the shaded region in dark red (inner) indicates the 95% confidence bands and shaded area in light red (outer) indicates the 95% prediction bands.

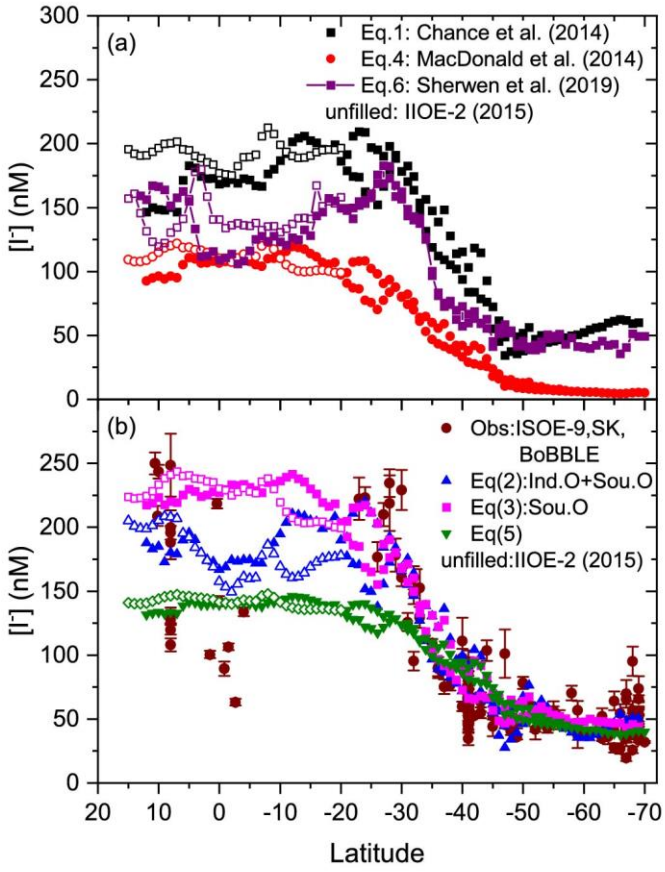
(a)
Eq.1: Chance et al. (2014)
Eq.4: MacDonald et al. (2014)
Eq.6: Sherwen et al. (2019)
unfilled: IIOE-2 (2015)
[I-] (nM)
(b)
Obs:ISOE-9,SK, BoBBLE
Eq(2):Ind.O+Sou.O
Eq(3):Sou.O
Eq(5)
unfilled:IIOE-2 (2015)
[I-] (nM)
Latitude

1084

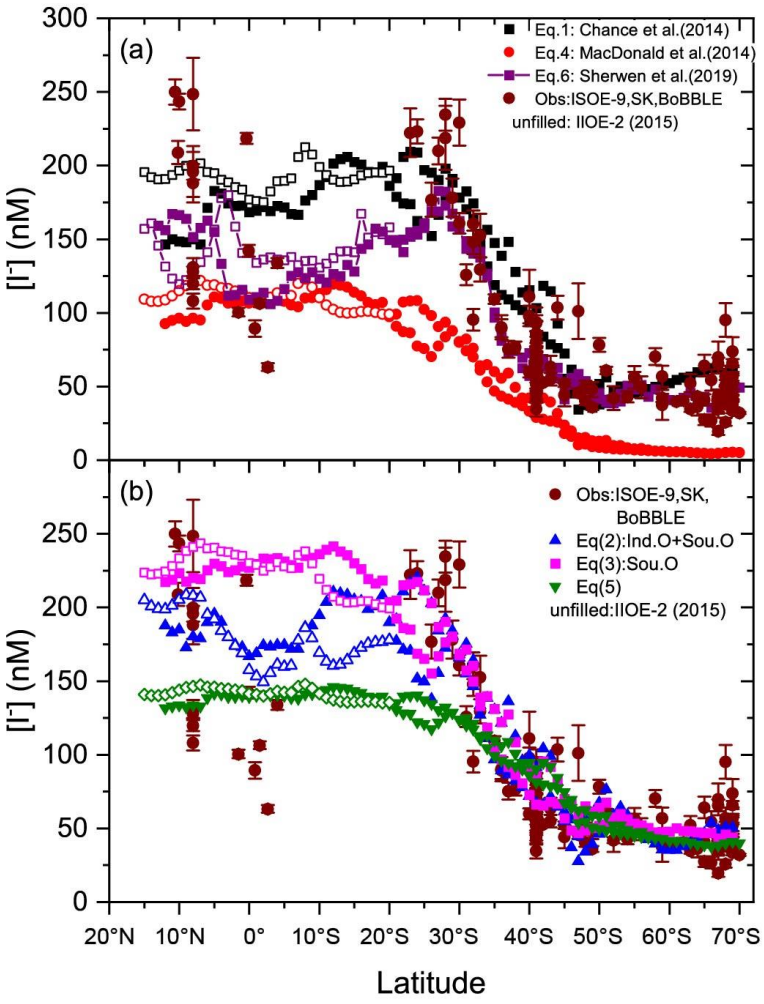

Figure 3: Latitudinal averages of calculated sea surface iodide (SSI) concentrations for each campaign using (a) existing, (b) new parameterisation tools and observations from ISOE-9, SK-333, and BoBBLE. Filled markers represent combined SSI from ISOE-8 and ISOE-9, unfilled markers represent SSI from IIOE-2 campaign.

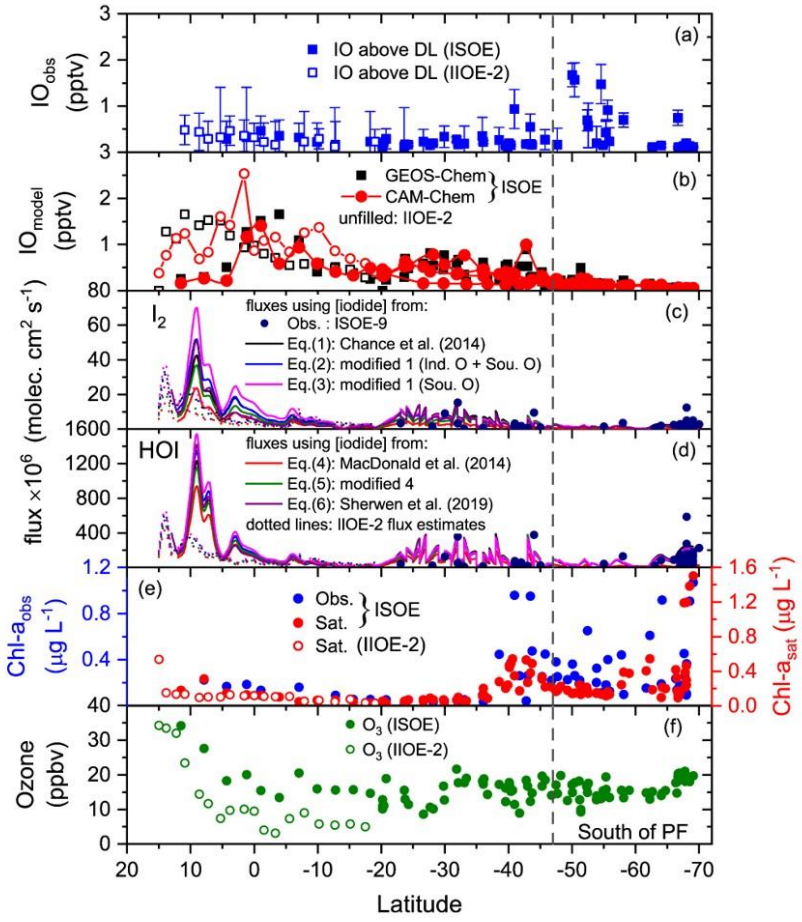
(a)
IO above DL (ISOE)
IO above DL (IIOE-2)
IO$_{obs}$ (pptv)
(b)
GEOS-Chem
CAM-Chem
ISOE
unfilled: IIOE-2
IO$_{model}$ (pptv)
(c)
I$_2$
fluxes using [iodide] from:
Obs. : ISOE-9
Eq.(1): Chance et al. (2014)
Eq.(2): modified 1 (Ind. O + Sou. O)
Eq.(3): modified 1 (Sou. O)
(d)
HOI
fluxes using [iodide] from:
Eq.(4): MacDonald et al. (2014)
Eq.(5): modified 4
Eq.(6): Sherwen et al. (2019)
dotted lines: IIOE-2 flux estimates
flux ×10^6 (molec. cm^2 s^{-1})
(e)
Obs.
Sat.
ISOE
Sat. (IIOE-2)
Chl-a$_{obs}$ (μg L^{-1})
Chl-a$_{sat}$ (μg L^{-1})
(f)
O$_3$ (ISOE)
O$_3$ (IIOE-2)
Ozone (ppbv)
South of PF
Latitude

1091

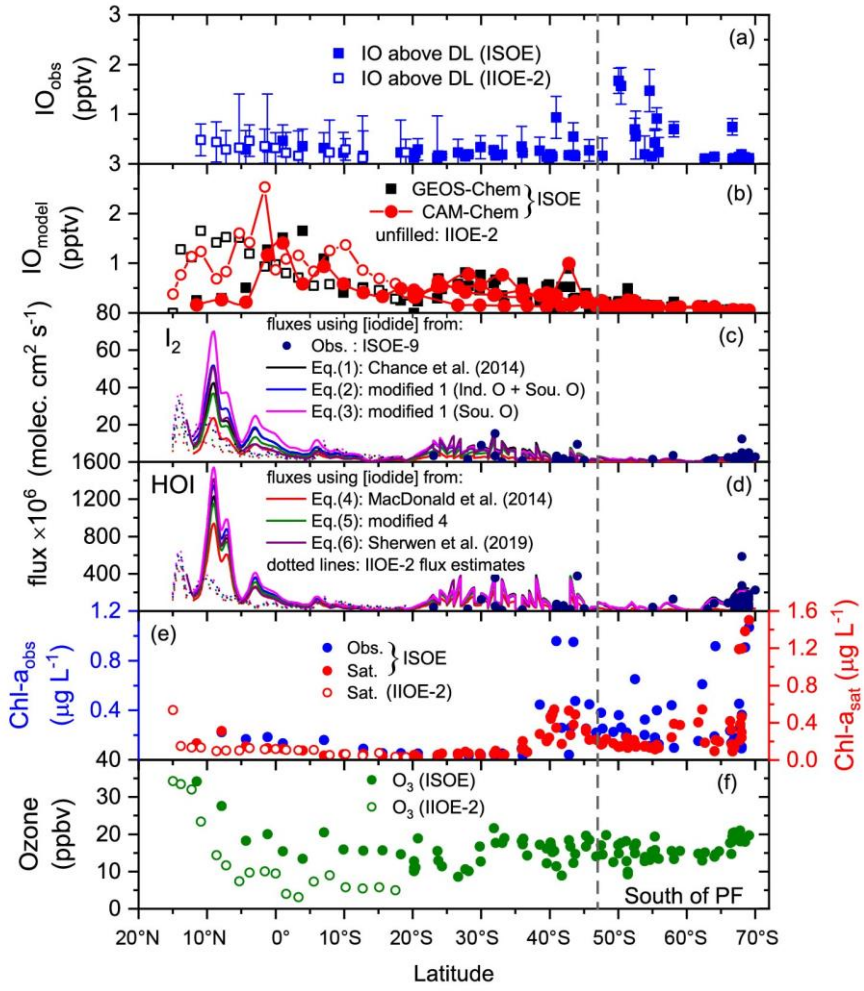

Figure 4: Daily averaged atmospheric and oceanic parameters combined from ISOE-8, IIOE-2, and ISOE-9 field campaigns. Data marked ISOE represents combined data from ISOE-8 and ISOE-9. Unfilled markers and dotted lines show values for IIOE-2. (a) IO above detection limit from ISOE-8, ISOE-9 and IIOE-2. (b) Surface IO values from GEOS-Chem and CAM-Chem models. (c) and (d) comprise of HOI and I_2 fluxes estimated from Eq. (7) and (6) respectively. Fluxes are colour coded for different sea surface iodide (SSI) datasets used for their estimation. Colours black, blue, red and green correspond to fluxes calculated using SSI estimation from Eq. (1) to (5), purple colour represents the use of model SSI predictions (Sherwen et al., 2019b)**, filled circles in dark blue correspond to measured SSI from ISOE-9 for each observation, (e) chlorophyll-*a***

observations from ISOE-8 and ISOE-9 (blue circles) and satellite data for all campaigns (red circles). (f) ozone mixing ratios from campaigns ISOE and IIOE-2. The dashed line marks the polar front at 47° S. Observational plots for ISOE-8 and IIOE-2 were adapted from Mahajan et al. 2019 a & b. The vertical dashed line through the figure indicates the PF (Polar Front).

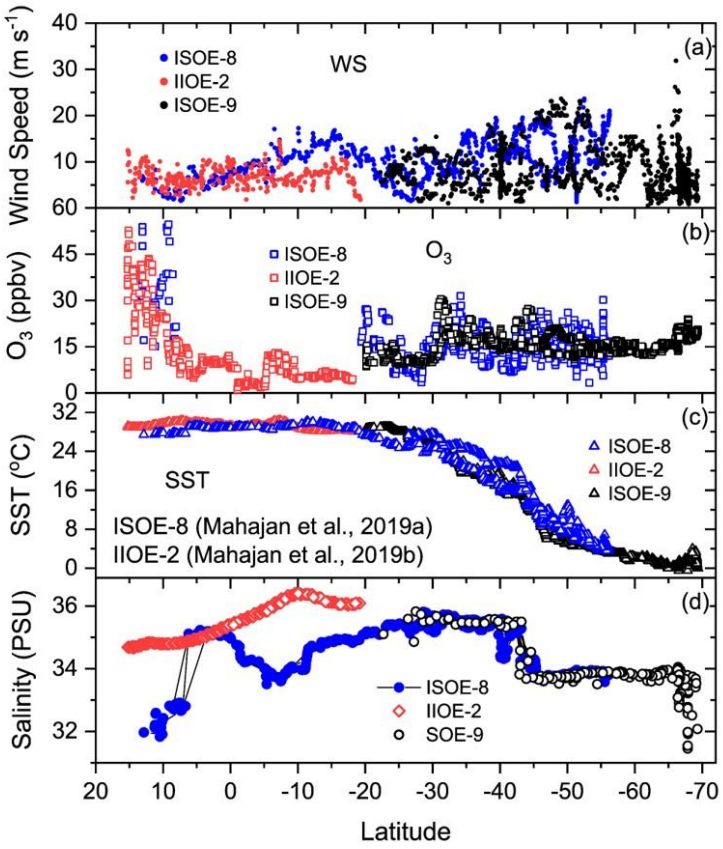
Wind Speed (m s-1)
ISOE-8
IIOE-2
ISOE-9
WS
(a)
O3 (ppbv)
O3
(b)
SST (°C)
SST
(c)
ISOE-8 (Mahajan et al., 2019a)
IIOE-2 (Mahajan et al., 2019b)
Salinity (PSU)
SOE-9
(d)
Latitude

1109

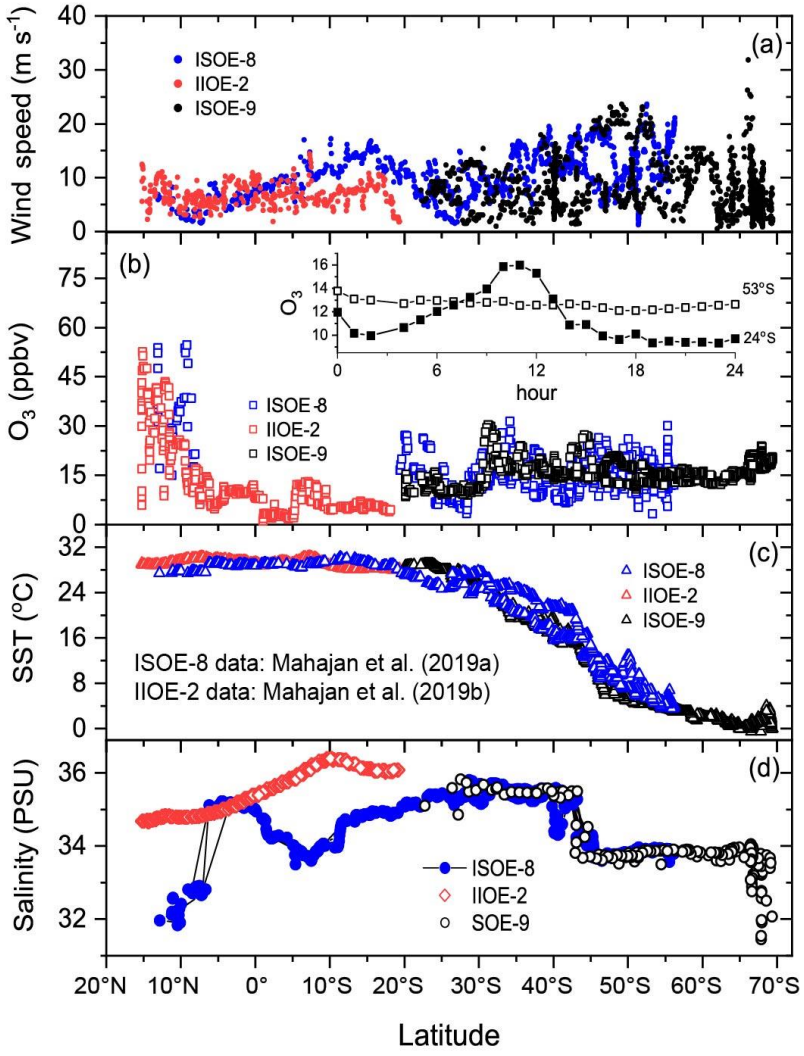

Figure 5: Latitudinal plot of hourly-averaged field measurements of wind speed, ozone mixing ratios, SST and salinity[†] from ISOE-8, IIOE-2, and ISOE-9 campaigns. Data

[†] Salinity data for IIOE-2 are monthly climatological means from World Ocean Atlas as described in the supplementary text.

markers in red belong to the IIOE-2 campaign; those in blue belong to the ISOE-8 and markers in black are from ISOE-9 for all the panels. Observational plots for ISOE-8 and IIOE-2 were adapted from Mahajan et al. 2019 a &b.

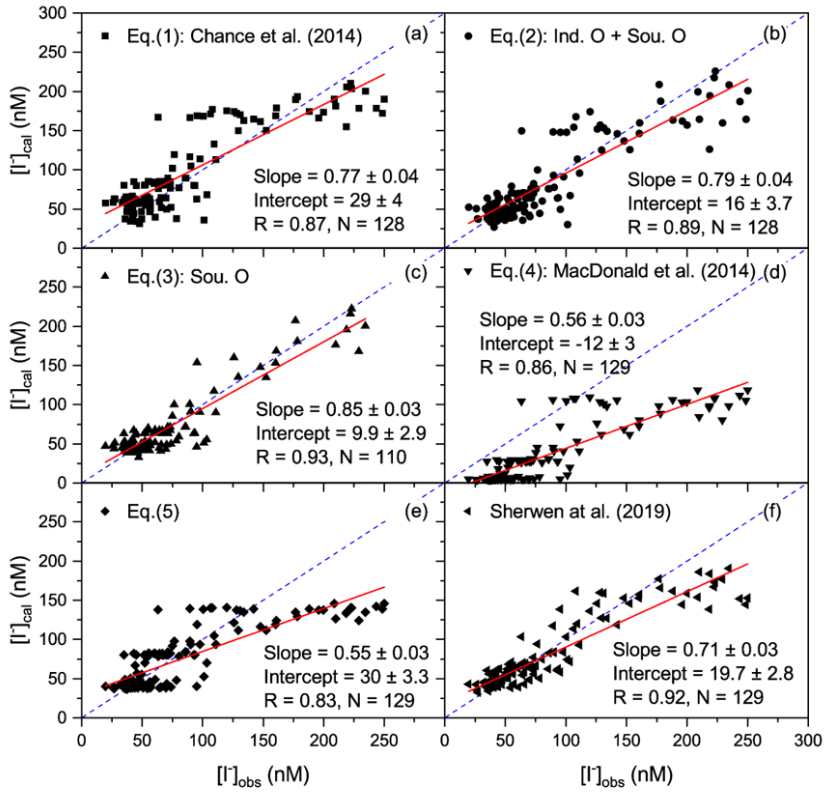

Figure 6: Linear fit analysis of estimated sea surface iodide (SSI) concentrations (y axis) from parameterisation methods in Eq. (1) to (5) and model prediction (Sherwen et al., 2019) against measured SSI concentration (x axis) from ISOE-9, SK-333 and BoBBLE. In panel (c) SSI are compared only with ISOE-9 observations for Southern Ocean specific parameterisation. R represents Pearson's correlation coefficient and N is the size of the dataset. Dashed blue line represents identity (1:1) line.

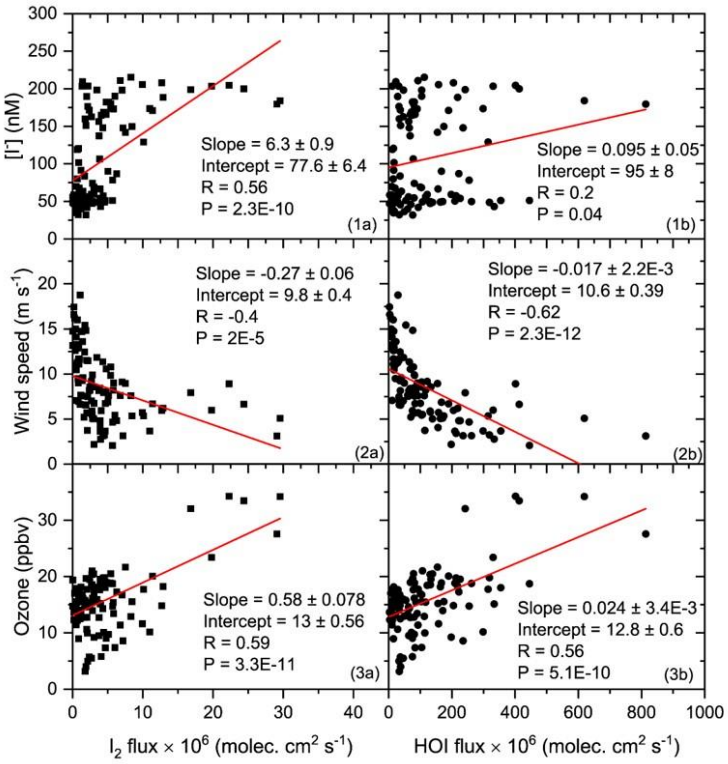

Figure 7: Linear fit of daily average sea surface iodide (SSI) concentration, wind speed and ozone mixing ratio (y axis) against calculated I_2 and HOI flux (x axis) against for all the campaign. HOI and I_2 are calculated using SSI estimated using the modified Chance parameterisation for Indian Ocean and Southern Ocean in Eq. (2).

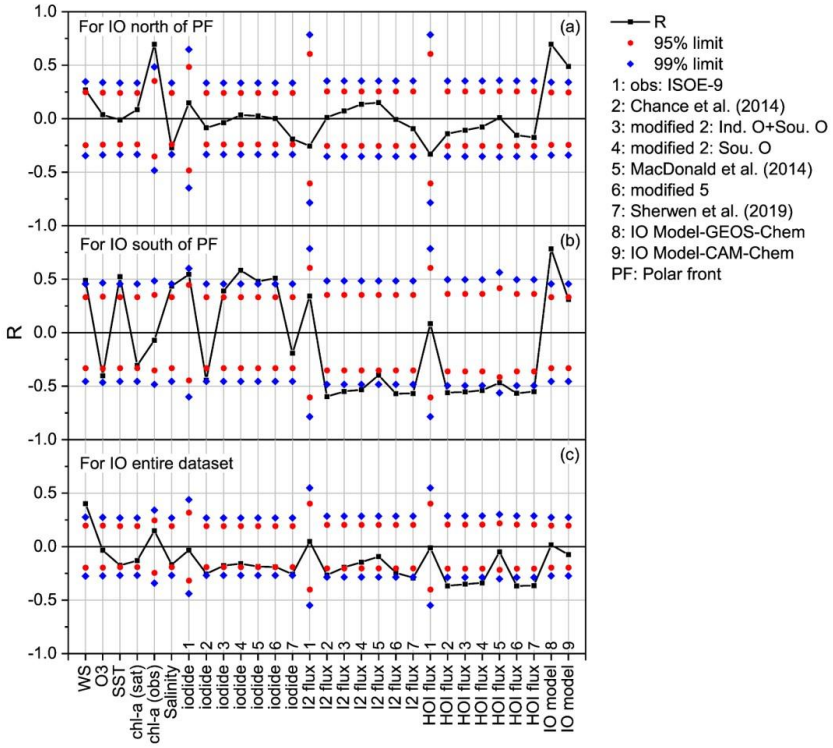

Figure 8: Pearson's correlation coefficient of observed iodine monoxide (IO) with oceanic and atmospheric parameters combined for ISOE-8, IIOE-2, and ISOE-9 campaigns. Correlations are performed for daily averages of IO and corresponding parameters listed on the X axis. The black squares represent Pearson's correlation coefficients (R), the diamonds (blue) mark the 99% confidence limit, and the circles (red) correspond to the 95% confidence limits in all the panels, (a) includes data from all campaigns to the north of the polar front (PF) (n = 72), (b) represents combined data for the south of the polar front (n = 48), the last panel (c) includes the entire dataset from three campaigns (n = 120).

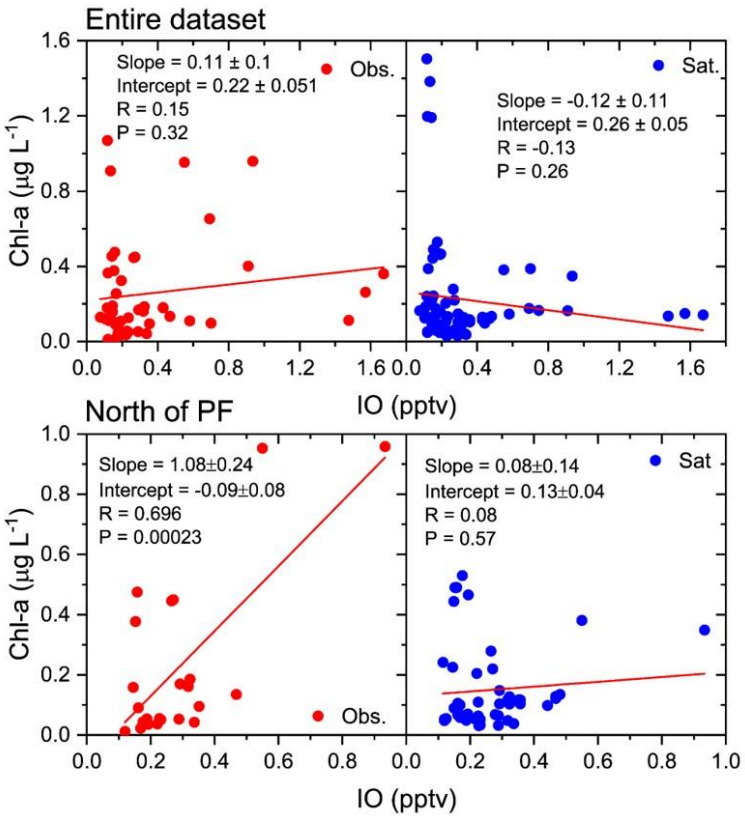

Figure 9: Linear fit of daily averaged field observations of chlorophyll-*a* (red circles) and chlorophyll-*a* satellite data (blue circles) (y axis) against observed iodine monoxide (IO) (x axis) from ISOE-8, IIOE-2, and ISOE-9 campaigns. The top panel includes chlorophyll-*a* for the entire dataset; the bottom panel includes data to the north of the polar front.

Formatted: Font color: Red

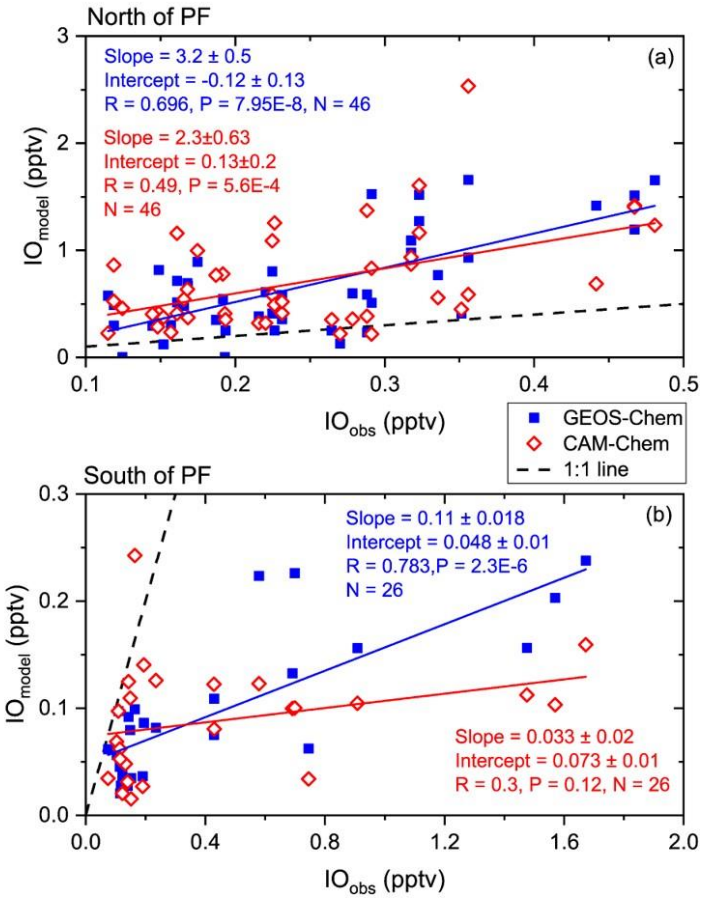

Figure 10: Linear fit of daily averages of modelled surface iodine monoxide (IO) output (y axis) from GEOS-Chem (filled blue squares) and CAM-Chem (unfilled red diamonds) against observed IO (x axis) for ISOE-8, IIOE-2 and ISOE-9 campaigns. (a) includes linear fits of both GEOS-Chem and CAM-Chem for IO detected to the north of the polar front, (b) shows the same for the region south of the polar front. Two data points in panel (a) at 41º S and 43º S are removed due to large differences between observation and modelled values.

10. Tables

Expedition	Research Vessel	Duration	Location	Meridional Transect	Observations
8th Indian Southern Ocean Expedition (ISOE-8)	Sagar Nidhi, India	7 Jan 2015 to 22 Feb 2015	Indian Ocean from Chennai, India to Port Louis, Mauritius	13º N to 56º S	IO, O_3
2nd International Indian Ocean Expedition (IIOE-2)	Sagar Nidhi, India	4 to 22 Dec 2015	Indian Ocean from Goa, India to Port Louis, Mauritius	15º N to 20º S	IO, O_3
Bay of Bengal Boundary Layer Experiment (BoBBLE)	R.V. Sindhu Sadhana	23 June 2016 to 24 July 2016	Southern Bay of Bengal	8º N to 10º N	Seawater samples for I^-
Sagar Kanya-333 (SK-333)	Sagar Kanya, India	5 Sept 2016 to 20 Sept 2016	Southern Arabian Sea and Southern Bay of Bengal	1.6º N to 4º S	Seawater samples for I^-
9th Indian Southern Ocean Expedition (ISOE-9)	S A Agulhas, South Africa	6 Jan 2017 to 26 Feb 2017	Indian and Southern Ocean from Port Louis, Mauritius to Antarctica	20º S to 70º S	IO, O_3, I^-

Table 1: Details of the three expeditions contributing to the IO and seawater iodide dataset in this study. Expeditions are listed in chronological order from 2015~~4~~ to 2017~~6~~.

Eq. No	Database location	Reference	Parametric equation ([iodide] in nM)	Data points	R^{2*}	R
Eq. (1)	*Majorly Atlantic and Pacific Ocean*	*Chance et al. (2014)*	$[iodide] = 0.28(\pm0.002) \times sst^2 + 1.7(\pm0.2) \times \lvert latitude\rvert + 0.9(\pm0.4) \times [NO_3^-] - 0.02(\pm0.002) \times MLD_{pt} + 7(\pm2) \times salinity - 309(\pm75)$	*n = 673*	*0.676*	*0.758*
Eq. (2)	Indian and Southern Ocean	This study	$[\text{iodide}] = 0.36(\pm0.04) \times sst^2 - 2.7(\pm0.5) \times \lvert\text{latitude}\rvert + 0.28(\pm0.57) \times [\text{NO}_3^-] + 0.64(\pm0.17) \times \text{MLD}_{\text{pt}} - 5.4(\pm3.82) \times \text{salinity} + 22(\pm137)$	n = 128	0.794	0.794^
Eq. (3)	Southern Ocean	This study	$[\text{iodide}] = 0.25(\pm0.017) \times sst^2 - 0.6(\pm0.4) \times \lvert\text{latitude}\rvert + 2.2(\pm0.4) \times [\text{NO}_3^-] - 5.5(\pm3.3) \times \text{salinity} + 212(\pm123)$	n = 110	0.859	0.859^
Eq. (3a)	Indian Ocean	This study	$[\text{iodide}] = 4.56(\pm6.45) \times \lvert latitude\rvert - 23.7(\pm31) \times salinity + 944(\pm1096)$	n = 18	0.325	NA
Eq. (4)	*Atlantic, Central and West Pacific Ocean*	*MacDonald et al. (2014)*	$[iodide] = 1.46 \times 10^{15} \times exp\left(\frac{-9134}{SST}\right)$	*n = ~88*	*0.71*	*0.739*
Eq. (5)	Indian and Southern Ocean	This study	$[\text{iodide}] = 3.6 \times 10^7 \times \exp\left(\frac{-3763}{SST}\right)$	n = 129	0.702	0.697^
Eq. (6)	*Atlantic, Pacific, Indian and Southern Oceans*	*Sherwen et al. (2019)*	*Machine learning based regression approach*	*n = 1293*	*-NA*	*0.842*

Formatted Table

Table 2: List of existing global (italics) and new region-specific (regular) parameterisations for sea surface iodide concentration indicating data location and number of data points used to formulate each equation. Here [iodide] represents sea surface iodide concentration in nM, sea surface temperature as 'sst' in ºC, and SST in K. Nitrate concentration ($[NO_3^-]$) is given in µM~~mol L^{-1}~~, mixed layer depth as MLD_{pt} in m, subscript 'pt' indicates potential temperature implying a temperature change of 0.5 ºC from the ocean surface (Monterey and Levitus, 1997), and salinity in PSU. Further details on individual parameters and the choice of Eq. (1) over others proposed in Chance et al. (2014) are discussed ~~further~~ in the supplementary text. R^{2*} represents the initial coefficient of determination (COD) while deriving each parameterisation, and R^2 represents COD from correlation analysis of the calculated iodide with observations in this study (ISOE-9, SK-333, BoBBLE).

^**Higher R^2 values for the modified parameterisations reflect the fact that they have been derived using the same observational data as they are tested on.**

Supplementary Material for 'Estimation of Reactive Inorganic Iodine Fluxes in the Indian and Southern Ocean Marine Boundary Layer'

Swaleha Inamdar[1,2], Liselotte Tinel[3], Rosie Chance[3], Lucy Carpenter[3], P. Sabu[4], Racheal Chacko[4], Sarat C. Tripathy[4], Anvita U. Kerkar[4], Alok K. Sinha[4], P. V. Bhaskar[4], Amit Sarkar[4,5], Rajdeep Roy[6], ~~Tomas~~ Tomás Sherwen[3,7], Carlos Cuevas[8], Alfonso Saiz-Lopez[8], Kirpa Ram[2] and Anoop S. Mahajan[1]*

[1]Centre for Climate Change Research, Indian Institute of Tropical Meteorology, Ministry of Earth Sciences, Dr Homi Bhabha Road, Pashan, Pune, 411 008, India

[2]Institute of Environment and Sustainable Development, Banaras Hindu University, Varanasi, 221005, India

[3]Wolfson Atmospheric Chemistry Laboratories, Department of Chemistry, University of York, YO10 5DD, UK

[4]National Centre for Polar and Ocean Research, Goa, 403 804, India

[5]Environment and Life Sciences Research Centre, Kuwait Institute for Scientific Research Centre, Al-Jaheth Street, Shuwaikh, 13109, Kuwait

[6]National Remote Sensing Centre, Department of Space Government of India Balanagar, Hyderabad, 500 037, India

[7]National Centre for Atmospheric Science, University of York, York YO10 5DD, UK

[8]Department of Atmospheric Chemistry and Climate, Institute of Physical Chemistry Rocasolano, CSIC, Madrid, Spain.

* corresponding author: Anoop S. Mahajan (anoop@tropmet.res.in); phone: +91 20 2590 4526

Supplementary Text

1. Abbreviations used in the text:

ISOE-8	8th Indian Southern Ocean Expedition
IIOE-2	2nd International Indian Ocean Expedition
ISOE-9	9th Indian Southern Ocean Expedition
SK-333	Sagar Kanya-333 expedition in the south Indian Ocean
BoBBLE	Bay of Bengal Boundary Layer Experiments
Chl-*a*	Chlorophyll-*a*
HYSPLIT	HYbrid Single-Particle Lagrangian Integrated Trajectory (HYSPLIT) model (Rolph et al., 2017; Stein et al., 2015)
DSCD(s)	Differential slant column density(ies)

2. Multiple linear regression analysis

A region-specific parameterisation tool for estimating sea surface iodide concentration was developed following the (Chance et al., 2014) method. Observations for SSI concentrations from ISOE-9, SK-333 and BoBBLE were used for the multiple linear regression analysis against various atmospheric and oceanic parameters. SST data used for linear regression analysis was recorded during ISOE-9 using a bucket thermometer at an interval of 6 hours accounting for a change of approximately 1 degree in the latitudinal track of the ship and simultaneously during each seawater iodide sampling. Seawater samples collected during ISOE-9 at the same interval as the recorded SST were used for salinity retrievals using the AUTOSAL salinometer. For the SK-333 and BoBBLE expeditions most of the samples were collected from the CTD casts and some (4 data points) were underway samples in case of

BoBBLE expedition. The MLD climatological monthly mean computed from climatological monthly mean profiles of potential temperature and potential density based on three different criteria was obtained using the World Ocean Atlas (Monterey and Levitus, 1997). That being; a temperature change from the ocean surface of 0.5 degree Celsius (MLD_{pt}), a density change from the ocean surface of 0.125 (sigma units) (MLD_{pd}), and a variable density change from the ocean surface corresponding to a temperature change of 0.5 degree Celsius (MLD_{vd}) (Monterey and Levitus, 1997). All three climatological monthly mean MLD data types (MLD_{pd}, MLD_{pt}, and MLD_{vd}) were used for linear regression with measured iodide concentration. The climatological monthly mean of sea surface nitrate concentrations for ISOE-9 was also obtained from the World Ocean Atlas 2013, version 2 (Garcia et al., 2013). Chl-*a* data for ISOE-9 was obtained from pigment analysis during ISOE-9.

3. Dataset used for SSI estimation

For estimating the SSI concentrations for all campaigns (ISOE-8, IIOE-2, and ISOE-9) using parameterisation methods in Eq. (1) to (5), the oceanic parameters were obtained from the observations during individual campaigns. Missing data was substituted with available data, as in the case of IIOE-2 campaign. For this campaign, salinity data was obtained from the World Ocean Atlas 2013, version 2 (Zweng et al., 2013). Also, chl-*a* data for IIOE-2 was obtained from level 3 daily and 8-day products of Aqua MODIS satellite (NASA-GSFC, 2017). Similarly, sea surface nitrate concentrations and MLD for all the campaigns were obtained from World Ocean Atlas (Garcia et al., 2013; Monterey and Levitus, 1997).

4. Parameterisation for SSI estimation

Chance et al. (2014) developed two versions of empirical relationship for SSI estimation. The first one is given in the main text (Eq. 1). For the regional specific modification (Eq. 2 and 3), each of the oceanic parameters was obtained for the same location (SST, salinity, chl-*a*) as

the measured SSI concentrations from ISOE-9, SK-333 and BoBBLE. Likewise, monthly climatological datasets were obtained for MLD and nitrate with a one-degree spatial resolution, as described in the previous section. The regression analysis for region-specific modification was initially divided in three sections – first for the all the SSI observations including the Indian Ocean and the Southern Ocean (ISOE-9, SK-333, and BoBBLE). The second only for the Southern Ocean region (ISOE-9) and lastly only the Indian Ocean region (SK-333 and BoBBLE). A list of adjusted R^2, slope, intercept and significance of all parameters for linear regression with observed iodide concentration is provided in Table S1. The third scenario ~~was rejected due to poor and~~resulted insignificant coefficient of determination values (R^2) for individual parameters. ~~The resulting parameterisation too was unable to fit the observations with predicted values for the Indian Ocean region.~~ In this case, ~~SST and~~ latitude and salinity were the only parameters that ~~correlated positively~~showed significant dependence on ~~to~~ the observed SSI (Table S1). Individual parameters with significant R^2 values were used to obtain a parametric equation for SSI concentration. The first, ~~and~~ second, and third scenario resulting in parametrisation denoted by Eq. (2), ~~and~~ Eq. (3), and Eq. (3a) respectively are~~is~~ given in the main text in Table 2. ~~A list of R^2, slope, intercept and significance of all parameters for linear regression with observed iodide concentration is provided in Table S1.~~ A combination similar to the Chance parameterisation given in Eq. (2) gave maximum R^2 value of 0.794 (N = 128) for the Indian Ocean and the Southern Ocean region. In this equation, all parameters are significant except for salinity and nitrate concentration. Removal of any one of these insignificant parameters did not make the other significant. The coefficient for this equation (Eq. 2) also remained insignificant with high error value (22 ± 137). The combination of SST^2, latitude, nitrate and salinity resulted in a maximum R^2 = 0.86 (N=110) for the dependent variable [iodide] in Eq. (3). The inclusion of MLD_{pt} (with highest R^2 for MLD) increased the R^2 slightly but had a non-uniform

Formatted: Superscript

distribution of the residuals and was thus excluded. Similarly, the addition of chl-*a* to the equation did not change the R^2 significantly, and thus chl-*a* was removed from the final equation. The Indian Ocean scenario parameterisation in Eq. (3a) obtained R^2 = 0.325 (N=18). All parameters (latitude, salinity) and the coefficient were insignificant with large error values as shown in Table 2. These equation datasets were tested for statistical robustness by ANOVA test using StatPlus analysis software. Both equation (2) and (3) dataset result in higher F ratio value corresponding to the critical F value from f-distribution table and p-value < 0.0001 at 0.05 significance level. Eq. (2) obtains F = 94 with (5, 122) degree of freedom (critical value = 2.289) and Eq. (3) obtains F = 161 with (4,105) degree of freedom (critical value = 2.458). However, Eq. (3a) Indian Ocean dataset provides statistically insignificant result as the F value 3.604 with (2,15) degree of freedom is lower than the critical value of 3.682 with p = 0.053. Thus, this parameterisation is omitted from further analysis in the study and is indicative that the sea surface iodide estimation in the Indian Ocean does not follow the Chance parameterisation technique. It is important to note that this analysis involved a small dataset (N=18) and more observational studies will be required to estimate iodide concentrations in this region. SSI concentration was also estimated using the logarithmic parameterisation by Chance et al. (2014) and it was found to be ~~very~~ higher in comparison to the measured SSI concentration from ISOE-9. The ln[iodide] equation estimated SSI concentrations of ~500 nM in the Indian Ocean region which is very high compared to global observations of SSI in the Indian Ocean (Chance et al., 2014, Chance et al., 2019) and in comparison to the observations from SK-333 and BoBBLE for the South Indian Ocean. Therefore, we excluded the logarithmic parametrization for this study and suggest that the ln[iodide] parametrization is not adequate for SSI estimation.

Formatted: Superscript

5. References

Chance, R., Baker, A. R., Carpenter, L. and Jickells, T. D.: The distribution of iodide at the

sea surface, Environ. Sci. Process. Impacts, 16(8), 1841–1859, doi:10.1039/C4EM00139G, 2014.

Garcia, H. E., Locarnini, R. A., Boyer, T. P., Antonov, J. I., Baranova, O. K., Zweng, M. M., Reagan, J. R. and Johnson, D. R.: WORLD OCEAN ATLAS 2013 Volume 4: Dissolved Inorganic Nutrients (phosphate, nitrate, silicate), NOAA Atlas NESDIS 76., 2013.

Monterey, G. and Levitus, S.: Seasonal Variability of Mixed Layer Depth for the World Ocean. [online] Available from: http://www.nodc.noaa.gov, 1997.

NASA-GSFC: Ocean Color Web. [online] Available from: https://oceancolor.gsfc.nasa.gov/, 2017.

Rolph, G., Stein, A. and Stunder, B.: Real-time Environmental Applications and Display sYstem: READY, Environ. Model. Softw., 95, 210–228, doi:10.1016/j.envsoft.2017.06.025, 2017.

Stein, A. F., Draxler, R. R., Rolph, G. D., Stunder, B. J. B., Cohen, M. D. and Ngan, F.: Noaa's hysplit atmospheric transport and dispersion modeling system, Bull. Am. Meteorol. Soc., 96(12), 2059–2077, doi:10.1175/BAMS-D-14-00110.1, 2015.

Zweng, M. M., Reagan, J. R., Antonov, J. I., Locarnini, R. A., Mishonov, A. V., Boyer, T. P., Garcia, H. E., Baranova, O. K., Johnson, D. R., Seidov, D. and Biddle, M. M.: WORLD OCEAN ATLAS 2013 Volume 2: Salinity. [online] Available from: http://www.nodc.noaa.gov/OC5/indprod.html, 2013.

6. Figures

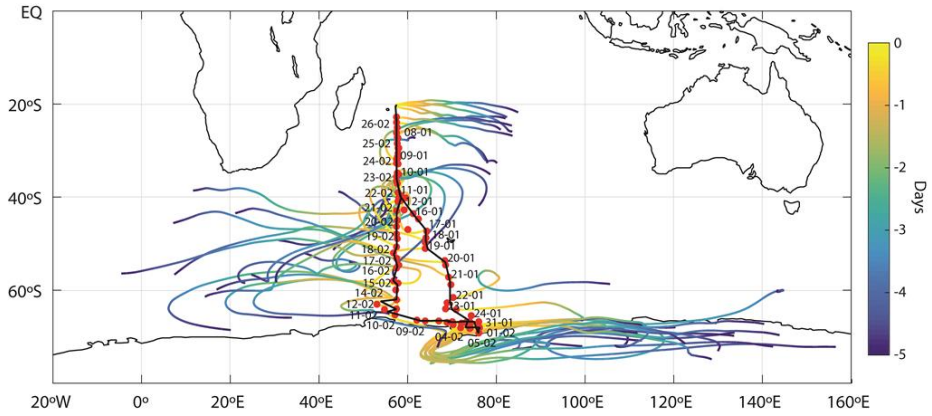

139

140 **Figure S1: Map of the south Indian Ocean and the Southern Ocean showing the cruise**
141 **track (black line) for the ISOE-9 campaign. Along the cruise track 5-days backward**
142 **wind trajectories (HYSPLIT) of the air masses arriving the locations at noon each day**
143 **of the ISOE-9 expedition. Sea surface iodide sampling locations marked in red circles**
144 **along with the date of sampling.**

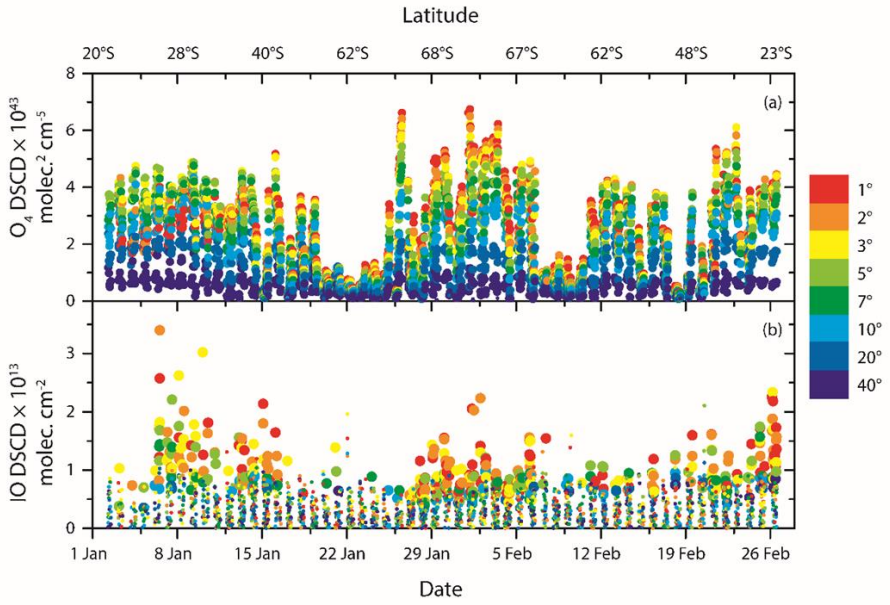

145

146 **Figure S2: Timeline of the O_4 and IO DSCDs observed during the ISOE-9 expedition.**
147 **The top scale indicates corresponding latitudes for the dates, and colour code represents**
148 **the elevation angle (°) for each scan. Smaller circles indicate DSCDs below σ detection**
149 **limit for IO and 2σ in case of O_4; bigger circles indicate DSCDs above the detection**
150 **limit respectively.**

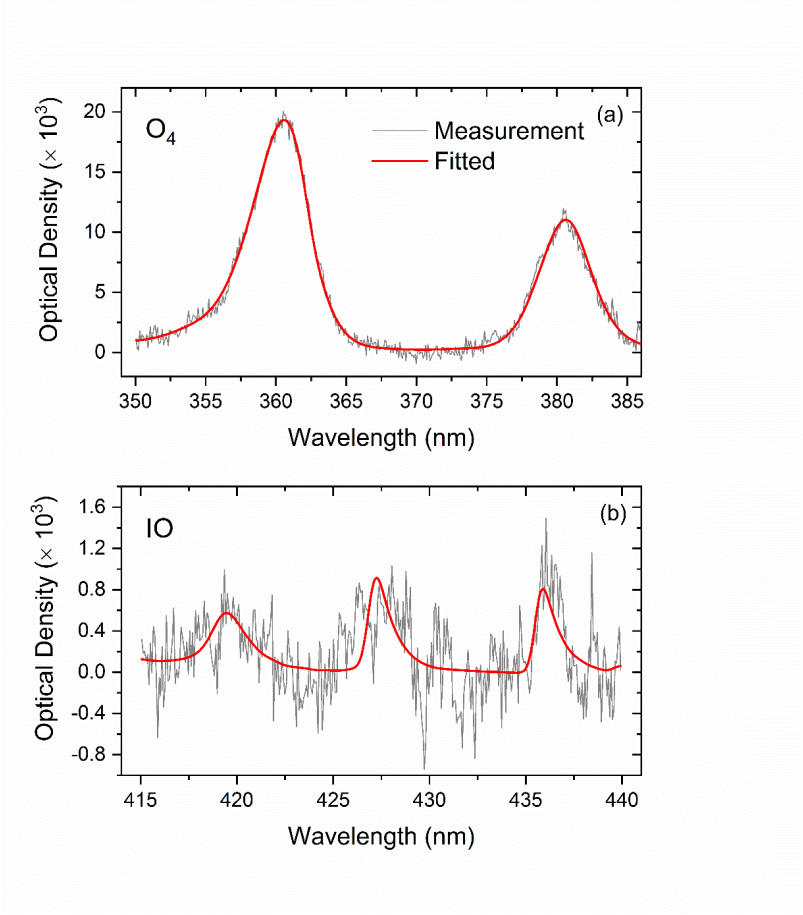

Figure S3: An example of typical spectral fit for O_4 (a) and IO (b) during the ISOE-9 expedition. These spectral fits were taken on 26 February 2017 at 15:35 (local time), for solar zenith angle 69.5° and 1° elevation angle. These fits retrieved O_4 slant column density of $(4.35\pm0.035)\times10^{43}$ molecules cm^{-2} and $(2.24\pm0.36)\times10^{13}$ molecules cm^{-2} with residual optical density (root mean square) of $3.2\times10^{-4}$and 5.5×10^{-4} respectively.

7. Tables

Parameter	R^2	Slope (m)	Intercept (C)	p < 5%? (p)
SST	0.64	4.26 ± 0.29	31 ± 4.77	Yes (0)
	0.62	*4.03 ± 0.304*	*32.2 ± 4.17*	*Yes (0)*
	0.07	28.8 ± 26.22	-668.85 ± 754.52	No (0.29)
1/SST (K^{-1})	0.62	-345781 ± 23910	1297 ± 83.9	Yes (0)
	0.59	*-322918 ± 25302*	*1215 ± 89.5*	*Yes (0)*
	0.07	-2616459 ± 2392959	8826 ± 7926	No (0.29)
SST^2	0.73	0.16 ± 0.0085	41.1 ± 3.6	Yes (0)
	0.79	*0.18 ± 0.01*	*39.2 ± 2.7*	*Yes (0)*
	0.07	0.51 ± 0.45	-261.9 ± 375.2	No (0.28)
NO_3	0.42	-3.24 ± 0.34	125 ± 5.7	Yes (0)
	0.39	*-2.63 ± 0.32*	*110.6 ± 5.8*	*Yes (3.06×10^{-13})*
	0.03	19.34 ± 27	153 ± 17	No (0.48)
|Latitude|	0.55	-2.1 ± 0.17	178.3 ± 8.3	Yes (0)
	0.52	*-2.43 ± 0.22*	*196.1 ± 11.7*	*Yes (0)*
	0.30	8.74 ± 3.35	108.5 ± 23.11	Yes (0.02)
Monthly MLD_{pt}	0.17	-1.1 ± 0.22	125 ± 9.2	Yes (1.2×10^{-6})
	0.08	*-0.63 ± 0.21*	*97.6 ± 9.4*	*Yes (0.003)*
	0.14	-2.69 ± 1.68	203.41 ± 30.38	No (0.13)
Monthly MLD_{vd}	0.04	-0.48 ± 0.2	98 ± 8	Yes (0.03)
	0.003	*-0.11 ± 0.19*	*75.9 ± 7.5*	*No (0.56)*
	0.16	-2.69 ± 1.55	193.52 ± 23.6	No (0.10)
Monthly MLD_{pd}	0.12	-0.67 ± 0.16	110 ± 7.8	Yes (5.2×10^{-5})
	0.05	*-0.35 ± 0.15*	*87.1 ± 7.7*	*Yes (0.02)*
	0.15	-2.51 ± 1.52	194.8 ± 25	No (0.12)
Salinity	0.08	16 ± 4.8	-468 ± 165	Yes (0.001)
	0.23	*21.8 ± 3.8*	*-675 ± 130*	*Yes (8×10^{-8})*
	0.30	-42.41 ± 16.21	1609.3 ± 551	Yes (0.02)

Chlorophyll *-a*	0.025	-37 ± 26	84 ± 8.6	No (0.16)
	0.002	*-7 ± 20*	*62 ± 7*	*No (0.73)*
	0.01	77.83 ± 206	136 ± 31	No (0.71)

Table S1: Linear regression analysis results for each parameter against field observations of sea surface iodide for paramterisation Eq. (2) in standard font and Eq. (3) in italics, and grey shaded rows for Eq. (3a). R^2 represents the coefficient of determination (COD); the last column is a check for statistical significance at 5% with the p-value in parenthesis.